







RESEARCH ARTICLE

High-resolution mapping of the global silicate weathering carbon sink and its long-term changes

Chaojun Li^{1,2}  | Xiaoyong Bai^{1,3}  | Qiu Tan⁴ | Guangjie Luo⁵ | Luhua Wu¹ | Fei Chen¹  | Huipeng Xi¹ | Xuling Luo¹ | Chen Ran¹ | Huan Chen¹ | Sirui Zhang¹  | Min Liu¹ | Suhua Gong¹ | Lian Xiong^{1,4}  | Fengjiao Song^{1,4} | Biqin Xiao^{1,4} | Chaochao Du^{1,4} 

¹State Key Laboratory of Environmental Geochemistry, Institute of Geochemistry, Chinese Academy of Sciences, Guiyang, Guizhou Province, China

²University of Chinese Academy of Sciences, Beijing, China

³CAS Center for Excellence in Quaternary Science and Global Change, Xi'an, Shanxi Province, China

⁴School of Geography and Environmental Sciences, Guizhou Normal University, Guiyang, China

⁵Guizhou Provincial Key Laboratory of Geographic State Monitoring of Watershed, Guizhou Education University, Guiyang, China

Correspondence

Xiaoyong Bai, State Key Laboratory of Environmental Geochemistry, Institute of Geochemistry, Chinese Academy of Sciences, Guiyang, 550081, Guizhou Province, China.
Email: baixiaoyong@vip.skleg.cn

Funding information

Western Light Cross-team Program Chinese Academy of Sciences, Grant/Award Number: xbzg-zdsys-202101; Western Light Talent Program (Category A), Grant/Award Number: 42077455; Western Light Talent Program, Grant/Award Number: 2018-99; Strategic Priority Research Program of the Chinese Academy of Sciences, Grant/Award Number: XDB40000000 and XDA23060100; Science and Technology Program of Guizhou Province, Grant/Award Number: 2022-198; Opening Fund of the State Key Laboratory of Environmental Geochemistry, Grant/Award Number: SKLEG2022206 and SKLEG2022208

Abstract

Climatic and non-climatic factors affect the chemical weathering of silicate rocks, which in turn affects the CO₂ concentration in the atmosphere on a long-term scale. However, the coupling effects of these factors prevent us from clearly understanding of the global weathering carbon sink of silicate rocks. Here, using the improved first-order model with correlated factors and non-parametric methods, we produced spatiotemporal data sets (0.25° × 0.25°) of the global silicate weathering carbon-sink flux (SCSF_α) under different scenarios (SSPs) in present (1950–2014) and future (2015–2100) periods based on the Global River Chemistry Database and CMIP6 data sets. Then, we analyzed and identified the key regions in space where climatic and non-climatic factors affect the SCSF_α. We found that the total SCSF_α was 155.80 ± 90 Tg C yr⁻¹ in present period, which was expected to increase by 18.90 ± 11 Tg C yr⁻¹ (12.13%) by the end of this century. Although the SCSF_α in more than half of the world was showing an upward trend, about 43% of the regions were still showing a clear downward trend, especially under the SSP2-4.5 scenario. Among the main factors related to this, the relative contribution rate of runoff to the global SCSF_α was close to 1/3 (32.11%), and the main control regions of runoff and precipitation factors in space accounted for about 49% of the area. There was a significant negative partial correlation between leaf area index and silicate weathering carbon sink flux due to the difference between the vegetation types. We have emphasized quantitative analysis the sensitivity of SCSF_α to critical factors on a spatial grid scale, which is valuable for understanding the role of silicate chemical weathering in the global carbon cycle.

KEYWORDS

carbon sink, climate change, modeling, rock weathering, silicate, spatio-temporal evolution

1 | INTRODUCTION

Silicate chemical weathering is considered to form a stable carbon sink on the geological time scale, and it effectively removes carbon dioxide from the atmosphere (CO_2), which is ultimately stored in the ocean as carbonate precipitation (Berner, 2006; Walker et al., 1981). Recent data analysis and modeling show that the negative feedback between silicate weathering and climate is also thought to modulate the recovery from transient carbon cycle perturbations on short timescales (Zeebe & Caldeira, 2008). There is also a negative feedback effect between silicate weathering and climate change on the scale of 10–100 years (Beaulieu et al., 2012). Therefore, a thorough study of the chemical weathering of silicate rocks is of great significance to the terrestrial carbon balance and the mitigation of global warming in the present and the future. Although relative to the chemical weathering of carbonate rocks, the weathering rate of silicate rocks is generally slower (Cao et al., 2018; Yan et al., 2012). Some scholars believe that the weathering rate of carbonate rocks is much greater than that of silicate weathering carbon sinks (about 15 times) (Zeng et al., 2019). However, the types of silicate rocks are diverse and they are widely distributed throughout the global land. Studies have shown that artificially accelerated weathering of silicate rocks can help offset the CO_2 emissions from human activities (Taylor et al., 2015; Vicca et al., 2022).

Many scholars have estimated the magnitude of the global silicate weathering carbon sink and the annual atmospheric CO_2 consumed by silicate weathering is about 0.118–0.169 Pg C (Gaillardet et al., 1999; Moon et al., 2014). However, there are significant differences in the data sources, resolution and estimation methods used in the various estimates. In addition to the traditional forward model and inversion model (Gaillardet et al., 1999; Moon et al., 2014), Hartmann (2009) used multiple linear regression methods to achieve the estimation of the silicate weathering carbon sink based on spatial grid data such as lithology, runoff (q), temperature (T), and soil properties on a global grid-scale. A particularly important consideration in the estimation is the quantification of soil shielding effects, which are determined by the difference in soil thickness caused by the physical erosion rate between flat areas and steep terrain (Stallard, 1995). The existing shielding factor is mainly based on the soil types as defined by the Food and Agriculture Organization system, and the soil types with an obvious soil shielding effect (e.g., Ferralsols, Acrisols, Nitisols, Lixisols, Histosols, and Gleysols) are used to set the shielding coefficient (the best value is set to 0.1), while soil types of other regions are ignored. This has led to a predictable result: the soil shielding effect in tropical regions may be underestimated, whereas in temperate and some subtropical regions, the soil shielding effect may vary greatly and may be overestimated (Hartmann et al., 2014b). However, the soil shielding effect can be replaced by physical erosion because most of the soil shielding effect comes from the erosion system. In this system, chemical weathering mainly occurs in the "supply limited" area, that is, when the physical erosion rate is low, thick soil will inhibit the chemical weathering rate (West,

2012). Therefore, the physical erosion rate has a non-negligible effect on chemical weathering. The current estimation of the physical erosion rate is mainly based on the suspended matter flux, which is affected by various factors such as climate, topographic slope, and land-use change (Gislason et al., 2009). Although there have been many outstanding studies on the physical erosion rate at the global scale, there is still a relative lack of relevant studies on the grid scale needed to achieve high resolution and a long time series. Maffre et al. (2018) have used T and q databases based on the Climate Research Unit (CRU) database to predict the global physical erosion rate. However, due to the complexity of the impact of human activities, the impact of human activities on physical erosion has not been considered on the spatial grid scale. Therefore, it might be possible to improve the estimation method of the physical erosion rate based on global land-use data sets, which is also very important for accurately quantifying the global silicate weathering carbon sink.

Due to the continuous development of the Global Coupled Model Intercomparison Project (CMIP), it is possible to widely use spatial data such as climatic and hydrological data with different high resolutions around the world. At the same time, there has been a more comprehensive and detailed compilation of the global river hydro-chemistry database (Hartmann et al., 2014a), and the global lithology map has been updated and improved (Hartmann et al., 2012). The data conditions for realizing the current and future simulations of global silicate rocks seem to be available. However, quantifying how carbon sequestration will change in the future is still a complex task for most models, mainly due to the coupling relationship between climate, hydrology, land use, and biogeochemical reactions (Hilton & West, 2020; Kump et al., 2000; White & Blum, 1995; Zhang et al., 2022a) and also because the models must be able to simulate a rapidly changing system under transient conditions (Godderis et al., 2013). Nevertheless, a current comprehensive analysis of these factors is still lacking, and the main control regions of the effect of different factors on silicate weathering carbon sinks have not been effectively clarified.

In this study, we optimized the calculation model of the global silicate weathering carbon sink (called "Improved first-order model with correlated factors") by quantifying the global soil shielding effect. On this basis, we mainly used the Global River Chemistry Database, high-resolution meteorological, ecological, and hydrological CMIP6 model data to assess the global silicate weathering carbon sink magnitude and its temporal and spatial evolution from 1950 to the end of this century. The ultimate purpose was to reveal the effect of different factors on the carbon sink of silicate weathering and to quantify the relative contribution rates and the main control regions within the spatial scale. In-depth analysis of the sensitivities of global silicate weathering carbon sinks to different primary controlling factors is important for understanding the future change process of silicate weathering carbon sinks. Under the severe situation of global warming, the research on carbon capture and storage, including the enhancement of silicate weathering carbon sinks, will help different countries or regions around the world to achieve carbon neutrality goals.

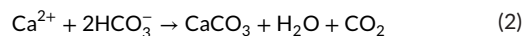
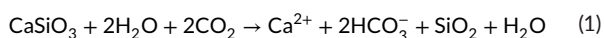
2 | MATERIALS AND METHODS

2.1 | Data collection and processing

The data sets collected and compiled in this study mainly include the following parts: (1) Hydro-chemical data from 6012 sites (about 120,000 samples) in the Global River Chemistry Database (1960–2010) (Hartmann et al., 2014b) and global river discharge database (GEMS-GLORI) (Meybeck & Ragu, 2012). The collected ions data mainly contains bicarbonate ions and chloride ions. For details, see the Methods section. (2) Grid data (runoff (q), temperature (T), precipitation (P), surface soil moisture content (SMC), evapotranspiration (ET), leaf area index [LAI]) in CMIP6 (Phase 6 of the Coupled Model Intercomparison Project) from 1950 to 2100 (<https://esgf-node.llnl.gov/search/cmip6>). According to the simulation experiment settings, these data are divided into the present period (1950–2014) and future period (2015–2100) with 2014 as the boundary. The future simulation data (2015–2100) involves four scenarios, namely SSP1-2.6, SSP2-4.5, SSP3-7.0, and SSP5-8.5 (Eyring et al., 2016). We compiled the first output products of the models (r1i1p1f1). In addition, to compare and validate the data from different sources, we collected other product data sets (Table S1) within different temporal scales. (3) Global 30 Arc-Second Elevation (GTOPO30) (1 km resolution) was from USGS EROS Archive (<https://www.usgs.gov/centers/eros/>). This data was used to calculate the slope gradient factor in this study. (4) Land-use harmonization product (LUH2) (1950–2100), which were annual data sets with a resolution of 25 km (<https://luh.umd.edu/data.shtml>). There were two data types, namely LUH 2v2h and LUH 2v2f data, each of which includes 12 possible land-use states, for instance, separation of primary and secondary natural vegetation into forest and non-forest sub-types, pasture into managed pasture and range land, and cropland into multiple crop functional types. (5) Soil types were obtained from the Harmonized World Soil Database (Version 1.2), and were publicly available from the Food and Agriculture Organization of the United Nations (FAO) (<http://www.fao.org/>). (6) Globally updated lithology data (Hartmann & Moosdorf, 2012), with a spatial resolution of $0.5^\circ \times 0.5^\circ$. Based on this data, this study extracted global silicate lithology data (11 types) (Figure S1). To facilitate analysis, we resample all global scale raster data to 25 km.

2.2 | Chemical principle of carbon sink estimates from the weathering of silicate rocks

Chemical weathering of silicate rocks is considered to be a stabilizer to regulate the global climate, and it is irreversible on the time scale of millions of years (Berner & Caldeira, 1997; Walker et al., 1981). This is mainly because it can remove atmospheric CO_2 to form bicarbonate (alkalinity), which flows into the ocean with the river, forms carbonate precipitation and stores carbon in the ocean (Berner et al., 1983; Mackenzie & Garrels, 1971).



The existing methods for calculating the carbon sink of the chemical weathering of silicate rocks (e.g., forward simulation, inversion simulation, multiple linear regression simulation) are mostly based on the data of river water chemistry data to calculate the flux of main ions, including main anions (HCO_3^- , Cl^- , SO_4^{2-} , NO_3^-) and cations (Ca^{2+} , Mg^{2+} , Na^+ , K^+). Through the enormous research and efforts of scholars, the global hydro-chemical data including data for the main cation and anion ions have been continuously improved. The latest global hydro-chemical data are published in the Global River Chemistry Database. The classic reaction Equation (1) suggests that chemical weathering of silicate rocks can generate calcium ions. In fact, the composition of silicate rocks or minerals is complex, and their weathering reactions can also generate other major cations (Mg^{2+} , Na^+ , and K^+). In theory, the anions and cations produced by the weathering of silicate rocks are in equilibrium. If the impacts of other factors including cation exchange are not considered, the sum of the main cations' concentrations produced by silicate weathering can be equivalent to that of the bicarbonate concentrations. In this way, the flux of HCO_3^- (FHCO_3^-) produced by the weathering of silicate rock could be used as an important indicator to evaluate its weathering effect.

However, the HCO_3^- concentrations measured directly in rivers have various sources, such as atmospheric deposition and human activities, exogenous acids (such as sulfuric acid and nitric acid), and even trace carbonate minerals in areas where silicate rocks are widely distributed. Sea salt correction (mainly using Cl^-) can remove the effects of atmospheric deposition and human activities, and this method has been widely used in most studies (Keene et al., 1986; Wilson, 1975). Therefore, bicarbonate ions and chloride ions are the key ions considered in this study. The removal of any other remaining effect factors needs to consider RCO_2 , which represents the ratio of atmospheric CO_2 consumed by the weathering of silicate rocks to the observed HCO_3^- concentration. At present, RCO_2 values have been calculated by basin-scale methods, considering that silicate rock weathering is affected by exogenous acids such as sulfuric acid and nitric acid other than carbonic acid, as well as the non-negligible trace amount of carbonate minerals (Kanzaki et al., 2020; Liu & Han, 2020; Torres et al., 2014). In addition to lithology, RCO_2 values are spatially heterogeneous due to the combined effects of various environmental factors (Bufe et al., 2021). Unfortunately, the current calculation of RCO_2 values is still at the global average level. Therefore, the in-depth research and accurate quantification of silicate weathering carbon flux still face challenges.

2.3 | Improved first-order model with correlated factors

The first-order model with correlated factors has been applied to the estimate of silicate weathering carbon sink (Hartmann et al.,

2014b). However, the difference from the traditional study is that this study adopts the random forest method (Breiman, 2001) instead of multiple linear regression. The random forest regression algorithm (RF) was chosen to simulate the bicarbonate ions flux (FHCO_3^-). Because RF is considered to be a more robust predictive model in the machine learning model (Bastin et al., 2019; Cotton et al., 2016), and it has been well applied in inverting ion activity coefficients (Li et al., 2018, 2019). Main environmental characteristics such as runoff, temperature and precipitation are used to explain some of the observed changes in bicarbonate ions flux (Godderis et al., 2009; Hartmann, 2009). Therefore, we constructed a random forest model with multiple environmental variables (q, T, P, ET, SMC, partial pressure of soil carbon dioxide ($p\text{CO}_2$) and LAI) to predict FHCO_3^- , and used the classic 10-fold cross-validation method to compare the model performance. The FHCO_3^- model is expressed as follows.

$$(\text{FHCO}_3^-)_k = \text{Average}\left(\sum_i^N h_i(x_k|(f_i))\right) \quad (3)$$

wherein $(\text{FHCO}_3^-)_k$ refers to the prediction result of the FHCO_3^- at different sites k in the overall prediction samples. $\text{Average}(\cdot)$ refers to the spatial average. $h_i(\cdot)$ refers to the prediction result of the decision regression tree. N refers to the number of stations. $x_k|(f_j)$ refers to the samples composed of the input samples (x_k) of the station (k) and the feature factor set (f_j) corresponding to the station. j refers to the number of feature factors.

In addition, combined with soil shielding factor (Hartmann et al., 2014b), and the ratio of atmospheric CO_2 consumed by silicate rocks weathering to the observed HCO_3^- concentration (RCO_2), we can estimate the global silicate rock weathering carbon sink flux (SCSF) from 1950 to 2100. Although current modeling studies as well as field observation studies suggest that the values of RCO_2 will change with the surface environment (such as erosion rate) and have certain spatial heterogeneity (Ferrier & Kirchner, 2008; Li et al., 2014). However, considering the complexity and time inconsistency of the collection of different rock samples around the world and the outstanding research work of previous studies (Börker et al., 2019; Hartmann, 2009; Moosdorf et al., 2011), the published and representative RCO_2 values were finally selected in this study instead of repeated calculation of the results. The calculation model of SCSF is as follows.

$$\text{SCSF} = \delta \cdot (\text{RCO}_2)_w \cdot \text{Average}\left(\sum_i^N h_i(x_k|(f_i))\right) \quad (4)$$

In the formula, SCSF refers to the flux of silicate weathering carbon sink ($\text{t C km}^{-2} \text{ yr}^{-1}$). δ refers to the soil shielding factor. RCO_2 values are detailed in Table S2. And w refers to each silicate rock type, such as granite, basalt, metamorphic rock, and sandstone.

Previous studies have shown that physical erosion can reflect the soil shielding effect to a certain extent (West, 2012; West et al., 2005). This study attempted to predict the physical erosion rate optimized by land use (ELU) of a long time series. Then, considering that the density of different rocks and minerals varies

significantly (Martin et al., 2019), the average rock density is assumed to be 2.7 kg m^{-3} in this study. The ELU was converted to the corresponding erosion thickness (mm kyr^{-1}) and normalized. To effectively represent the soil shielding effect, we performed a cosine-triangular transformation on the converted physical erosion thickness and the final range is between 0 and 1. The converted raster data was used as the new soil shielding factor (δ_α). Finally, the calculation method of the global silicate weathering carbon-sink flux (SCSF_α) was optimized. The SCSF_α calculation model is as follows.

$$\text{SCSF}_\alpha = \delta_\alpha \cdot (\text{RCO}_2)_w \cdot \text{Average}\left(\sum_i^N h_i(x_k|(f_i))\right) \quad (5)$$

2.4 | Accuracy evaluation methods

To avoid over-fitting of the RF model, we chose cross-validation (CV) methods. The recommended 10-fold CV was used here (Kohavi, 1995; Wong, 2015). The data processing of this study was carried out in R software. The results were evaluated through three indicators, namely correlation coefficient (R), root mean square error (RMSE), and mean absolute error (MAE) (Kuhn, 2008). The final calculated accuracy values were the average of all CV accuracy values.

Furthermore, we verified the effectiveness of the spatial grids of the simulation results. We have chosen the spatial efficiency metric (SPAEF) here, originally proposed by Demirel et al. (2018). This indicator is mainly used for spatial pattern comparison of observed and simulated variables and has been effectively used in distributed hydrological modeling (Herrnegger et al., 2020; Koch et al., 2018). The calculation formula of this indicator is as follows.

$$\text{SPAEF} = 1 - \sqrt{(R(O,S) - 1)^2 + \left(\frac{CV_O}{CV_S} - 1\right)^2 + (HM(O,S) - 1)^2} \quad (6)$$

wherein SPAEF refers to spatial validity, and its value range is $[-\infty, 1]$. O stands for space observation data. S refers to spatial simulation data. R refers to the Pearson correlation coefficient. CV refers to the coefficient of variation. HM refers to histogram match. We normalized the observational and simulated spatial data.

2.5 | Physical erosion rate

The physical erosion rate algorithm used in this study is the BQART model (Syvitski & Milliman, 2007). The model is based on a global database of 488 rivers and aims to estimate the erosion flux of each river to the ocean. The deviation of the model is about 3%. Maffre et al. (2018) extended the model to the global spatial grid scale ($1^\circ \times 1^\circ$) and realized the estimation of the global multi-year average physical erosion rate. Based on the idea of spatialization, we estimated the spatial distribution map of the global physical erosion rate from 1950 to the end of this century. The calculation formula is mainly as follows.

$$E = \varphi \cdot q^{0.31} \cdot A^{-0.5} \cdot s \cdot \max(T, 2) \quad (7)$$

wherein E refers to the physical erosion rate ($\text{t km}^{-2} \text{ yr}^{-1}$). $\varphi = 6 \times 10^2$ (t yr^{-1}) (Syvitski & Milliman, 2007). q refers to the runoff depth (mm). A refers to the grid area (km^2). T refers to temperature ($^{\circ}\text{C}$). s refers to slope gradient, and the calculation formula of s is as follows.

$$s = \sqrt{\left(\frac{\partial h}{\partial x}\right)^2 + \left(\frac{\partial h}{\partial y}\right)^2} \quad (8)$$

In the formula, h refers to altitude (m), x refers to longitude, and y refers to latitude.

However, the interference of human activities is not considered in the calculation of the physical erosion rate. The global physical erosion rate is strongly affected by land-use change, and construction on land may have a restrictive effect on physical erosion. Land-use change is the dominant factor determining sediment yields and soil loss rates (Erskine et al., 2002; Luo et al., 2022). At present, high-resolution Land-Use Harmonization product data (LUH2) have been widely used. These conditions make land-use factors more convenient for calculation on a global grid scale.

Therefore, in view of the differences between the physical erosion rate under different land-use types, we revised the physical erosion rate and ultimately improved the estimation method of the physical erosion rate. Based on the land-use coordination data, the 12 types of land use were first merged into six types, namely forest land (f), grassland (g), crop land (c), urban land (u), bare land (b), and water body (w). It is worth noting that the LUH2 data do not include the changes in water bodies. This is mainly because the changes in water bodies (e.g., lakes and rivers) are very small. Therefore, in this study, we considered the multi-year average spatial distribution of water bodies. In summary, we will eventually improve the calculation model of the physical erosion rate was improved as follows.

$$\begin{aligned} \text{ELU} = & (1 - f_r(1 - f))E_f + (1 - g_r(1 - g))E_g + (1 - c_r(1 - c))E_c \\ & + (1 - u_r(1 - u))E_u + (1 - b_r(1 - b))E_b + (1 - w_r(1 - w))E_w \end{aligned} \quad (9)$$

wherein E_f , E_g , E_c , E_u , E_b , and E_w refer to the physical erosion rate ($\text{t km}^{-2} \text{ yr}^{-1}$) under the corresponding land-use type calculated by Equation (7). f_r , g_r , c_r , u_r , b_r , and w_r refer to the area ratio scores of the corresponding land-use types on the grid scale. f , g , c , u , b , and w refer to the soil conservation or soil erosion prevention practice factor under different land-use types. This idea mainly comes from the human activity management support practice factor in the general soil erosion model. This factor is an indicator for measuring the effectiveness of land management activities in reducing land loss in catchment areas (Borrelli et al., 2020; Yang et al., 2003). Based on this, the human activity management support factors of forest land, grassland, crop land, urban land, water body and bare land were 1, 1, 0.5, 0, 0, and 1 respectively. In summary, following simplification of Equation (9), the final physical erosion rate model was constructed as follows.

$$\text{ELU} = E_f + E_g + (1 - 1/2c_r)E_c + (1 - u_r)E_u + E_b + (1 - w_r)E_w \quad (10)$$

2.6 | Calculation method of partial pressure of soil carbon dioxide

$p\text{CO}_2$ is considered to be an important factor affecting the weathering carbon sink of silicate rocks (Gaillardet et al., 2019). It can control the saturation state with respect to minerals and the resulting mineral dissolution. It mainly comes from soil microbial activity and root respiration (Kuzakov, 2006; Miellnick & Dugas, 2000), which provides a source of CO_2 for silicate weathering. $p\text{CO}_2$ is accompanied by changes in the external environment (precipitation, temperature, microbial activity, etc.) showing obvious temporal and spatial variations (Reicosky et al., 2008). At present, there are three main methods for estimating $p\text{CO}_2$, which are related to temperature, actual ET, and SMC (Goderis et al., 2009; Gwiazda & Broecker, 1994). The method of estimating $p\text{CO}_2$ in this study is mainly derived from the study of Brook et al. (1983), which is considered to be a widely used method.

$$\log(p\text{CO}_2) = \log_{10}(p\text{CO}_2\text{atm}) + 2.09 \times (1 - e^{-0.00172ET}) \quad (11)$$

wherein the unit of $p\text{CO}_2$ is atm. ET (mm) refers to the actual ET. The ET data from CMIP6 is used in this study. ET is the flux of water into the atmosphere due to conversion of both liquid and solid phases to vapor from underlying surface and vegetation. The logarithm of atmospheric CO_2 partial pressure is -3.47 .

2.7 | Calculation method of partial correlation coefficients

There may be a correlation between any two environmental variables. We need to control other variables to avoid mutual interference between variables, so as to calculate the correlation coefficients between silicate weathering carbon sink and each variable more truly. Therefore, we chose the partial correlation analysis method (de la Fuente et al., 2005), and the main theoretical formulas are as follows.

$$R_1(x_n, y | x_1, x_2, \dots, x_m) = \frac{-c_{x_n y}}{\sqrt{c_{x_n x_n}} \sqrt{c_{y y}}} \quad (12)$$

wherein x refers to the eight main variables mentioned in this study (ET , ELU , LAI , P , q , SMC , $p\text{CO}_2$, and T), y refers to the global silicate weathering carbon-sink flux (SCSF_α). x_n refers to the n th variable among the variables. R_1 refers to the partial correlation coefficients of the partial correlation coefficients x_n and y , and c refers to the corresponding element in the inverse matrix of the correlation coefficient matrix. After calculating the partial correlation coefficients, we performed a t-test on the calculated result.

2.8 | Calculation method of relative contribution rate

On the spatial grid scale, the relative contribution rates of main factors to the SCSF_α were determined by referring to the following calculation method of contribution rate (Chen et al., 2020a).

$$\text{Contribution}_i = \frac{[f(i)]^2}{\sum_1^i [f(i)]^2} \times 100\%, \quad (i = 1, 2, 3 \dots 8) \quad (13)$$

wherein Contribution_i refers to the relative contribution rate of different factors $f(i)$ to the silicate weathering carbon sink, $f(i)$ refers to the eight main variables mentioned earlier in this article (ET, ELU, LAI, P, q, SMC, pCO_2 , and T).

2.9 | Determination of the main control regions of different factors

The relative spatial contribution rate of different factors can represent the effect of a single factor on the SCSF_α , but there is interaction or coupling influence mechanisms between different factors. Therefore, it is necessary to further clarify the main control regions of all factors in spatial grids. We calculate the contribution rates of the factor to the trend of the SCSF_α based on the partial correlation coefficients (equivalent to the partial derivative) multiplied by the slope of the factor itself (Roderick et al., 2007). Then, the overall trend (slope) is subtracted from the contribution values of all estimated factors to obtain the contribution values of the residual factor (OF). All the factor contribution values are bounded by 0, and the positive and negative contribution value regions are extracted respectively. The maximum value of the positive contribution value layer mainly comes from the positive contribution dominant factor, while the minimum value in the negative contribution value raster layer comes from the negative contribution dominant factor. We mapped the spatial distribution of the dominant positive and negative contribution factors. The relationships between the trend of silicate weathering carbon sink and the contribution rate of factors are as follows.

$$\frac{dy}{dt} = \sum_1^i \frac{\partial y}{\partial x_i} \times \frac{dx_i}{dt} + \frac{\partial y}{\partial x_0} \times \frac{dx_0}{dt}, \quad (i = 1, 2, 3 \dots 8) \quad (14)$$

wherein y refers to the global silicate weathering carbon-sink flux (SCSF_α). t refers to the study periods. x_i refers to eight factors (T, P, q, ET, SMC, pCO_2 , ELU, and LAI, respectively). x_0 refers to the residual factors (OF).

2.10 | Non-parametric methods

The spatial trend analysis of variables mainly used two non-parametric methods, namely, Sen's slope and Mann-Kendall trend test (Kendall & Stuart, 1968; Mann, 1945; Sen, 1968). Compared with the parametric test method, the non-parametric test methods do not require the tested sample data to follow a certain distribution and are not affected by anomalies. Therefore, these two methods are widely used in global change research (Deng et al., 2020; Song et al., 2022; Yang et al., 2019). The Sen's trend analysis method was proposed by Sen et al in 1968. This method was widely used

to study long-term series analysis. In addition, based on the Mann-Kendall test method, we tested the statistical significance levels of the trends.

2.11 | Monte Carlo error propagation method

In this study, we chose a general function for the calculation of uncertainty propagation by higher-order Taylor expansion, and Monte Carlo simulation including covariances. Uncertainty propagation is based completely on matrix calculus accounting for full covariance structure. Monte Carlo simulation is conducted using a multivariate t-distribution with covariance structure. Input data is the expression for estimating the SCSF_α and factors data based on summaries (mean and s.d.). Densities are derived from 100,000 Monte Carlo simulations. The calculation process is mainly implemented in R 4.0.3 using the "propagate" package.

3 | RESULTS

3.1 | Estimation of carbon sink magnitude

Based on the improved first-order model with correlated factors, we calculated the magnitude of the global silicate weathering carbon sink from 1950 to 2100. The SCSF_α from 1950 to 2014 was about $1.39 \text{ t C km}^{-2} \text{ yr}^{-1}$. The total flux of silicate chemical weathering carbon was about $155.80 \text{ Tg C yr}^{-1}$ (Table S2), equivalent to the carbon absorbed by 50 billion adult trees every year, which accounted for about 7.53% of the latest estimated value of forest carbon sink (about $2.07 \text{ Pg C yr}^{-1}$) (Harris et al., 2021). The average value of the SCSF_α under different scenarios in the future (SSPMean) was $1.57 \text{ t C km}^{-2} \text{ yr}^{-1}$, and the total flux was about $174.70 \text{ Tg C yr}^{-1}$. Compared with the total flux of the present period, the global silicate weathering carbon sink in future period is expected to increase by approximately $18.90 \text{ Tg C yr}^{-1}$ (12.13%).

Lithology is a key factor affecting the silicate weathering carbon sink (Mackenzie & Garrels, 1971; Suchet & Probst, 1995). It has a dominant controlling effect on dissolved products and may obscure the influence of other factors, such as climate. Therefore, we compared the flux and total flux of the weathering carbon sinks of 11 different types of silicate rocks (Table S2). We found that the flux of Pyroclastics (PY) ($3.17 \text{ t C km}^{-2} \text{ yr}^{-1}$) was higher than that of Basic volcanic rocks (VB) weathering carbon sink ($2.93 \text{ t C km}^{-2} \text{ yr}^{-1}$). Thus, PY had the fastest weathering rate among all silicate rocks. In this study, VB mainly refers to mainly basalt, which is currently widely believed to be the type of silicate rock with the highest weathering rate (Dessert et al., 2003; Ibarra et al., 2016; Louvat & Allègre, 1997). However, some research results have also emphasized the high chemical weathering rate of PY, which is mainly due to its high volcanic glass content and small grain size (Dahlgren et al., 1999; Hartmann & Moosdorf, 2011). Volcanic glass may also be a driving factor in the ratio of basalt to the total CO_2 consumed in silicate

weathering, although the area of basalt in the silicate rock is relatively small (Dessert et al., 2003). The global distribution area of PY (approximately 0.6%) is much smaller than that of VB (approximately 3.5%), which is about 5.83 times greater than that of PY. Therefore, the total flux of the VB weathering carbon sink is relatively large, which also shows that VB plays an important role in the silicate weathering carbon sink. Whether it is now or under different scenarios in the future, it can be found that the total flux of the weathering carbon sink of unconsolidated sediments (SU) and siliciclastic sedimentary rocks (SS) is much higher than that of other silicate lithologies, indicating that these two types of rocks have high carbon sequestration potential. This mainly depends on their extensive terrestrial distribution area, which respectively accounts for about 21% and 14% of the global land area (statistics deducting part of the carbonate area ratio).

3.2 | Temporal evolution trends

Combined with the variations in the main factors (Figure S2), we analyzed the temporal variations of the $SCSF_{\alpha}$ by the end of this century (Figure 1). We found that future periods were generally higher than the present period, especially after 2015, with a significant increase, which was closely related to the basic data sets of the simulation process (Figure S2). In particular, the $SCSF_{\alpha}$ showed an insignificant upward trend as a whole, and the current $SCSF_{\alpha}$ would change from an insignificant upward trend ($3.79 \times 10^{-4} \text{ t C km}^{-2} \text{ yr}^{-1}$) to an average insignificant downward trend in the future ($-1.47 \times 10^{-4} \text{ t C km}^{-2} \text{ yr}^{-1}$). However, the trend of $SCSF_{\alpha}$ under different scenarios in the future would be significantly different, which was not the same as the research finding that all future scenarios in the existing research showed an upward trend (Godderis et al., 2013). We found that SSP1-2.6 and SSP5-8.5 showed a significant downward trend, with slopes of $-2.08 \times 10^{-4} \text{ t C km}^{-2} \text{ yr}^{-1}$ ($p = .14$) and $-6.02 \times 10^{-4} \text{ t C km}^{-2} \text{ yr}^{-1}$ ($p < .001$), which could be mainly affected by the simulation results of physical erosion factors. Among them, the land-use change, the crop land change and these two scenarios have relatively similar change trends (Figure S3). SSP2-4.5 and SSP3-7.0 showed a significant upward trend, with slopes of $4.28 \times 10^{-4} \text{ t C km}^{-2} \text{ yr}^{-1}$ ($p < .01$) and $3.23 \times 10^{-4} \text{ t C km}^{-2} \text{ yr}^{-1}$ ($p < .05$).

The bicarbonate flux ($FHCO_3^-$) is an important factor for simulating the chemical weathering process of silicate rocks, and its magnitude is affected by many factors such as climate change factors and vegetation coverage (Raymond et al., 2008). Through machine learning inversion of $FHCO_3^-$, we found that although the anomaly values of $FHCO_3^-$ under different scenarios in present and future periods showed an increasing trend, the increasing anomaly rate in the future period was slower than the present period (Figure 1). ELU is another important factor affecting silicate chemical weathering besides $FHCO_3^-$ (Godderis et al., 2017; Maher & Chamberlain, 2014), and ELU mainly acts on it by influencing the soil shielding effect (Stallard, 1995). However, with the disturbance of human activities, land-use patterns (especially crop land and urban land) have

undergone significant changes (Figure S4), and this variation also affects the global carbon neutrality goal and the carbon cycle process (Achard et al., 2004; Tian et al., 2021; Zhang et al., 2022b). The ELU also affects the global silicate weathering carbon through changes in land use. The rate of ELU anomaly was from an insignificantly decreasing trend of $6.64 \text{ kg km}^{-2} \text{ yr}^{-1}$ ($p = .90$) during present period to a significant increasing trend of $410 \text{ kg km}^{-2} \text{ yr}^{-1}$ ($p < .001$) during mean future period (SSPMean) (Figure 1c). It was worth noting that the global ELU was showing a slight downward trend in the present period, which could be related to the construction of hydro-power stations and dams on many large rivers (Li et al., 2017). However, in future periods, due to the impact of climate change, the erosion rate was expected to show a significant increase trend.

3.3 | Spatial evolution patterns

To further quantify the spatial patterns and variation characteristics of the $SCSF_{\alpha}$ in different periods, we showed the global geographical distribution of the $SCSF_{\alpha}$ (Figure 2a) and main factors (Figure S3). The $SCSF_{\alpha}$ ranged from 0.01 to $24.08 \text{ t C km}^{-2} \text{ yr}^{-1}$, and its distribution had obvious spatial heterogeneity. The high-value areas were mainly distributed in Southeast Asia, central Africa, central and eastern parts of South America and North America, whereas the low-value areas were mainly concentrated in northern and southern Africa, and central Asia. In general, we found that 70% of the global total flux of the silicate weathering carbon sink came from about 30% of silicate distribution areas (Figure S5a). Among all silicate rock types, SU was the most widely distributed in the world. After deducting part of the carbonate content, it accounted for about 21% of the global land area. The total flux of carbon sink was primarily concentrated in areas with relatively good hydrothermal conditions, such as southern Asia. By comparing with rock weathering carbon sinks, the distribution concentration of silicate weathering carbon sink was weaker than the weathering carbon sinks of all rocks in the world (Hartmann et al., 2014). 70% of rock weathering carbon sinks were concentrated in 10% of the global land area. This was mainly subject to the concentration of non-silicate rocks, especially carbonate.

In addition, we calculated the spatial evolution trends of the $SCSF_{\alpha}$ (Figure 2) and main factors (Figures S6 to S15) from present period to different scenarios in future periods based on the Sen's slope, and performed Mann-Kendall test on them. We found that there was a relatively obvious increasing trend in the polar climate zone, especially in future scenarios of SSP2-4.5, SSP3-7.0 and SSP5-8.5. The Arctic Ocean coast area showed a significant increasing trend, which was mainly affected by future global warming (Figure S13). However, there was also a clear downward trend in some regions. The central regions of Africa shifted from a growth trend to a downward trend under different scenarios, which could be limited by future moisture conditions such as P and q in the regions (Figures S6, S9, S10). Although more than half (about 54%) of the global silicate weathering carbon sinks showed an upward trend

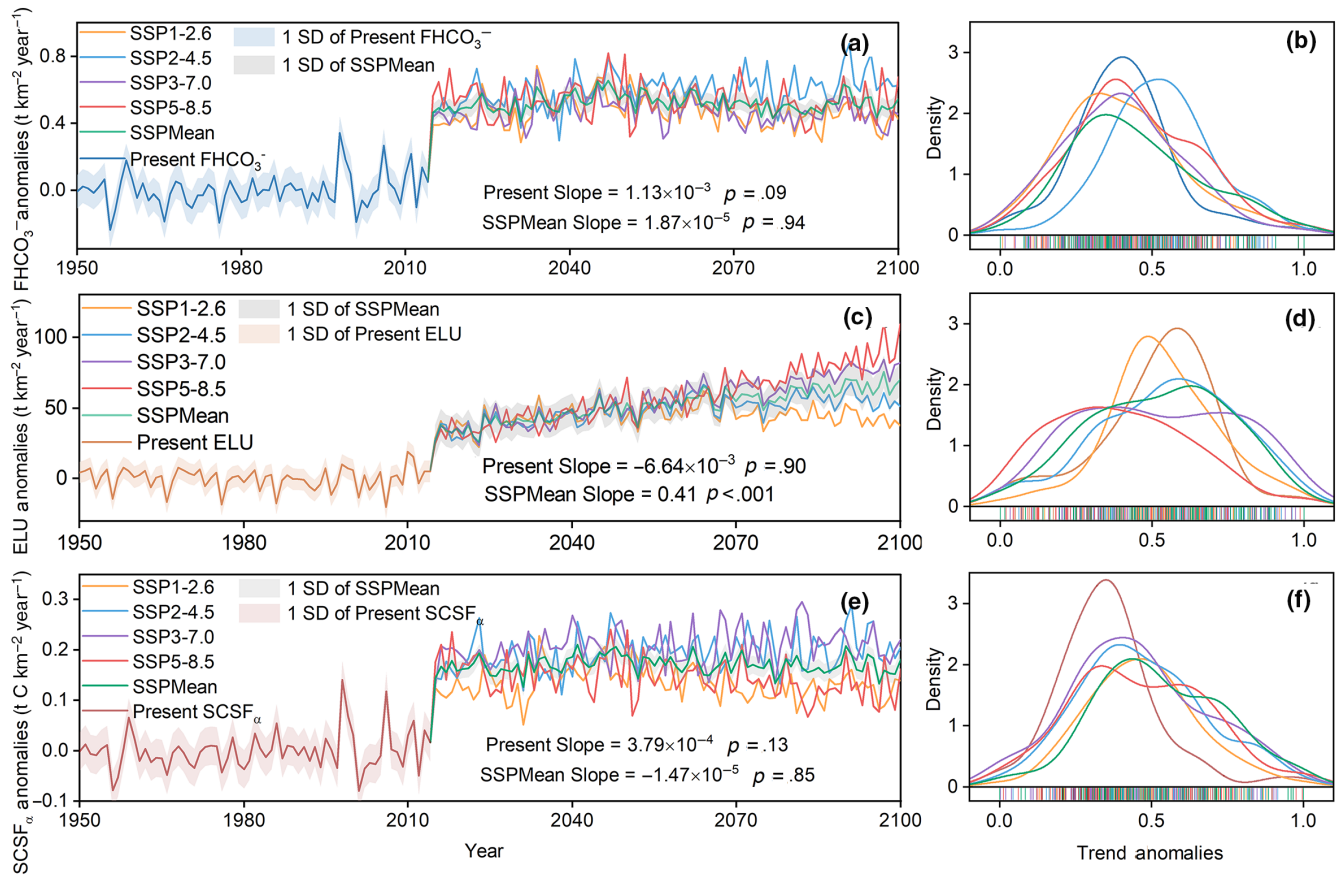


FIGURE 1 Anomaly trends of the time series from different variables. (a) The bicarbonate ions flux (FHCO_3^-). (b) Physical erosion rate optimized by land use (ELU). (c) The global silicate weathering carbon-sink flux (SCSF_α). SSPMean refers to the average value of the SCSF_α under different scenarios in the future (SSP1-2.6, SSP2-4.5, SSP3-7.0, and SSP5-8.5). (b), (d), and (f) refer to the normalized probability distribution of time anomaly values from FHCO_3^- , ELU, and SCSF_α , respectively [Colour figure can be viewed at [wileyonlinelibrary.com](https://onlinelibrary.wiley.com)]

($2.34 \times 10^{-3} \text{ t C km}^{-2} \text{ yr}^{-1}$) in the present period. Especially under the SSP2-4.5 scenario, the upward trend of the SCSF_α in about 57% of the area reached $3.00 \times 10^{-3} \text{ t C km}^{-2} \text{ yr}^{-1}$. However, under this scenario about 43% of the regions were still showing a clear downward trend, and the obvious decrease regions were mainly concentrated on the Black Sea coast and northwestern South America. This also implied that under the background of global warming, the evolution trend of silicate weathering carbon sinks was obviously regional.

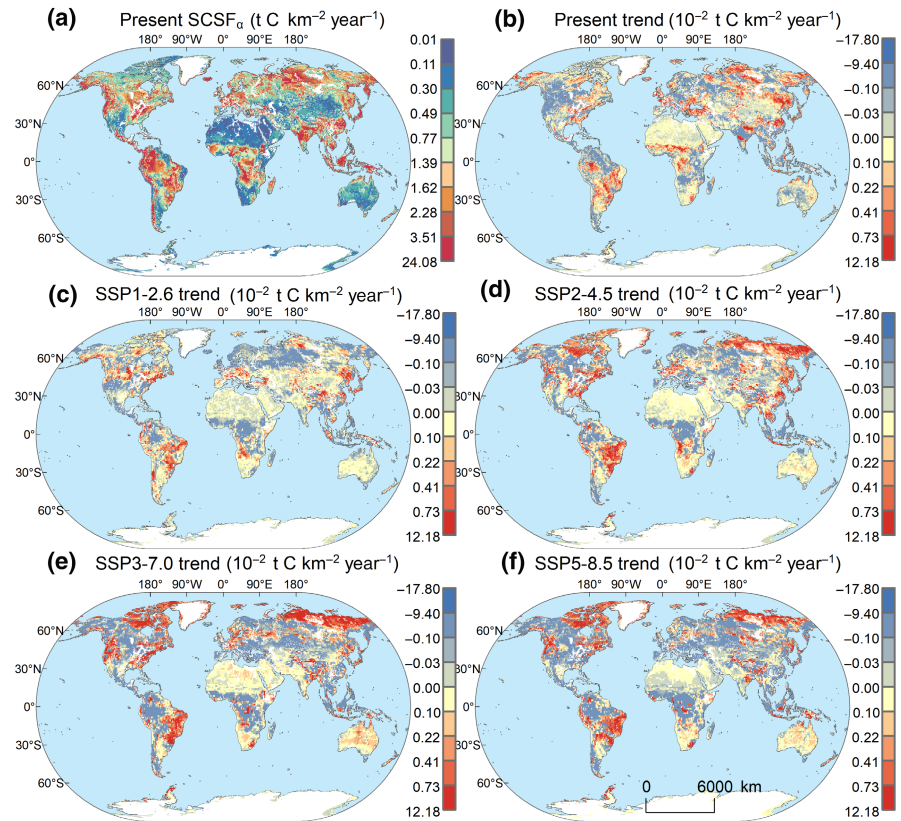
3.4 | Sensitivity to different controlling factors

Considering that the factors affecting the estimation of SCSF_α mainly come from FHCO_3^- , RCO_2 and soil shielding, the sensitivity of the change of SCSF_α to these three variables was tested in this study (Figure S5b). We found that the SCSF_α was much more sensitive to FHCO_3^- than the other two variables, and the sensitivity of the former was about 12 times that of the latter two. Moreover, the difference between the sensitivity of the SCSF_α to soil shielding and RCO_2 was small, and the former was slightly higher than the latter. These factors were affected by some relative factors. Specifically, RCO_2 values were mainly affected by lithology. The soil shielding

effect mainly changed with the change of ELU. FHCO_3^- was affected by q, P, T, and other meteorological and hydrological factors. To effectively quantify the relative spatial contribution rates of different factors to silicate weathering carbon sinks, we further analyzed the sensitivity of the SCSF_α to the primary factors. Because RCO_2 was mainly affected by lithological distribution, we assumed that the effect of this factor was relatively stable or basically unchanged. In this way, we focused on the factors related to FHCO_3^- and soil shielding effect, including eight main factors, namely ET, P, T, q, SMC, pCO_2 , ELU, and LAI.

Next, we analyzed the partial correlation between the main controlling factors and the SCSF_α in present period and further clarified the geographical distribution patterns of the regions with significant positive and negative partial correlations of these factors (Figure 3). In terms of the proportion of positive and negative correlations (Table S3), we found that the relationships between q, P, ELU, T, pCO_2 , and SCSF_α were dominated by significant positive and partial correlations, that was, these factors played a major role in limiting the SCSF_α . Of all the factors considered, the area proportion of the significant partial correlation was the largest for q, especially in the area of more than 86.57%, which further proves that this factor plays a major role in the weathering carbon sink of silicate rocks. It could

FIGURE 2 Spatial trends in the global silicate weathering carbon-sink flux ($SCSF_{\alpha}$) between present period (1950–2014) and future period (2015–2100). The future variations were estimated under SSP1-2.6, SSP2-4.5, SSP3-7.0, and SSP5-8.5 scenarios [Colour figure can be viewed at wileyonlinelibrary.com]



be seen from the latitude distribution that q was related to the $SCSF_{\alpha}$ and the correlation coefficient was also significantly higher than 0.5. The other factors (LAI, ET, and SMC) were dominated by significant negative partial correlation, of which the area of significant correlation of LAI was the smallest (14.24%) and was dominated by significant negative partial correlation. In addition, in terms of latitudinal distribution, P was associated with the $SCSF_{\alpha}$ in high latitudes. There was an obvious positive partial correlation between T and the $SCSF_{\alpha}$ in the low latitudes of the northern hemisphere (15°N–30°N).

However, SMC showed a significant negative correlation with the $SCSF_{\alpha}$ at high latitudes in the northern hemisphere. Meanwhile, temperature showed a significant positive correlation with $SCSF_{\alpha}$ at high latitudes, which indicates that the silicate chemical weathering in these regions was obviously limited by temperature. There was a significant negative partial correlation between LAI and $SCSF_{\alpha}$. We speculate that this is likely due to the fact that different vegetation types have different effects on the $SCSF_{\alpha}$. A study in the Isthmus of Panama showed that the weathering carbon flux of silicate rock had a significant positive correlation with forest cover but a negative correlation with cultivated land, grassland or shrub (Goldsmith et al., 2015). There was a significant negative partial correlation between ET and $SCSF_{\alpha}$, mainly in the tropical desert climate of Australia, which was strongly constrained by hydrological conditions.

In the spatial grid distribution, different factors not only had obvious differences in the partial correlation with the $SCSF_{\alpha}$ but also had different relative contribution rates to the $SCSF_{\alpha}$ (Figure 4). Nevertheless, we found that the regions with significant positive and partial correlation between the main factors and the $SCSF_{\alpha}$

became the regions with a high contribution rate of each factor to the $SCSF_{\alpha}$. As can be seen from the box diagram (Figure S16), q had the largest average contribution rate to the $SCSF_{\alpha}$, accounting for about 32.11%. Therefore, q explained the spatial variability of nearly one-third of the $SCSF_{\alpha}$ in the world. This implies the important dependence of the $SCSF_{\alpha}$ on the strength of the global water cycle. In addition, the relative contribution rate of SMC was about 16.22%, but it was mainly manifested in the negative contribution of high latitude, which was related to its significant negative partial correlation in this region. However, the relative contribution rate of LAI was the smallest (6.13%), which was consistent with the previous significant partial correlation between LAI and $SCSF_{\alpha}$ (Figure 3).

3.5 | Main control regions of different factors on spatial grids

We quantified the dominant contribution areas from different biophysical factors to global $SCSF_{\alpha}$, including the eight main factors mentioned above and the residual factor (OF) (Figure 5). Here, the OF refers to the effect factors for which it was difficult to obtain data or for which we could not realize global spatial grid simulation at present, such as water residence time, secondary minerals, landslide, and glacier melting (Calmels et al., 2007; Torres et al., 2016). We found that the positive contribution of P (30.27%) and q (18.77%) to the $SCSF_{\alpha}$ reached about 49% in the control regions. The main controlling role of these two factors could be clearly seen in the latitudinal distribution (Figure 5c).

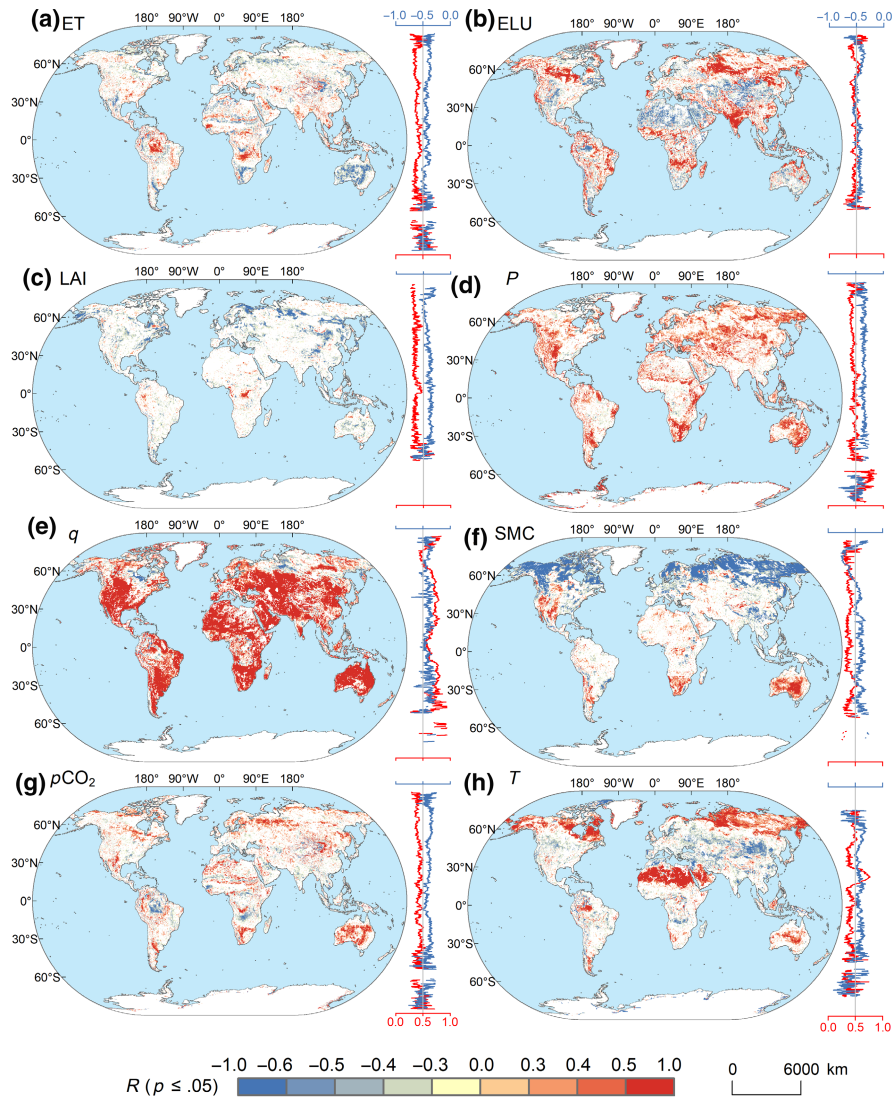


FIGURE 3 Sensitivity of the sensitivity of global silicate weathering carbon-sink flux to main factors. (a) ET (Evapotranspiration), (b) ELU (Physical erosion rate optimized by land use), (c) LAI (Leaf area index), (d) P (Precipitation), (e) q (Runoff), (f) SMC (Surface soil moisture content), (g) $p\text{CO}_2$ (Partial pressure of soil carbon dioxide), (h) T (Temperature). Based on t-test, the regions of significant partial correlation with $p \leq .05$ were counted. The blue line refers to the negative correlation distribution and the red line refers to the positive correlation distribution [Colour figure can be viewed at wileyonlinelibrary.com]

In the high latitudes of the southern hemisphere, the positive dominant role of P was the most obvious, which is generally consistent with the findings of previous studies (Ruddiman, 1997; White & Blum, 1995). In terms of the proportion of q area in the positive and negative contribution areas, the area proportion of negative main control regions (19.68%) was slightly larger than that of positive main control regions (18.77%). This was associated with the evolution trend of q in the present period and its partial correlation with the SCSF_α on the spatial scale. At the same time, compared with the proportion of the area of the positive main control regions, the area of P in the negative main control regions was significantly smaller. On the contrary, the area of negative main control regions of ET increased significantly, which also reflected the weakening effect of ET on the chemical weathering of silicate rocks. However, we found that regardless of whether it was a positive contribution area or a negative contribution area, the proportion of the control area of the LAI was the least (0.31–0.36%). This was similar to the previous lowest relative contribution rate of LAI. Although LAI had the least control area for the silicate rock weathering carbon sink, the impact of the vegetation on silicate rock weathering carbon sink was invalid

if it was ignored. In addition, the area of the negative contribution by the ELU factor (4.95%) was slightly larger than that of the positive contribution (4.10%).

4 | DISCUSSION

4.1 | Comparison with previous related studies

The average magnitude of the SCSF_α estimated here was compared with that reported by some previous studies based on multiple meteorological and hydrological data (Table S4) (Amiotte Suchet et al., 2003; Zhang et al., 2021). The ranges of the flux and total flux of the previous estimation results were $1.45\text{--}1.76 \text{ t C km}^{-2} \text{ yr}^{-1}$ and $41\text{--}169.52 \text{ Tg C yr}^{-1}$, respectively, and thus, the SCSF_α ($1.39 \text{ t C km}^{-2} \text{ yr}^{-1}$) estimated in this study was slightly lower than the values reported previously and the total flux ($155.80 \text{ Tg C yr}^{-1}$) was within the range of the values reported previously. However, there were significant differences between this study and other studies in terms of data compilation, methods, and spatial resolution of mapping. First of

FIGURE 4 Spatial distribution of relative contribution of different factors to silicate rock weathering carbon sink [Colour figure can be viewed at wileyonlinelibrary.com]

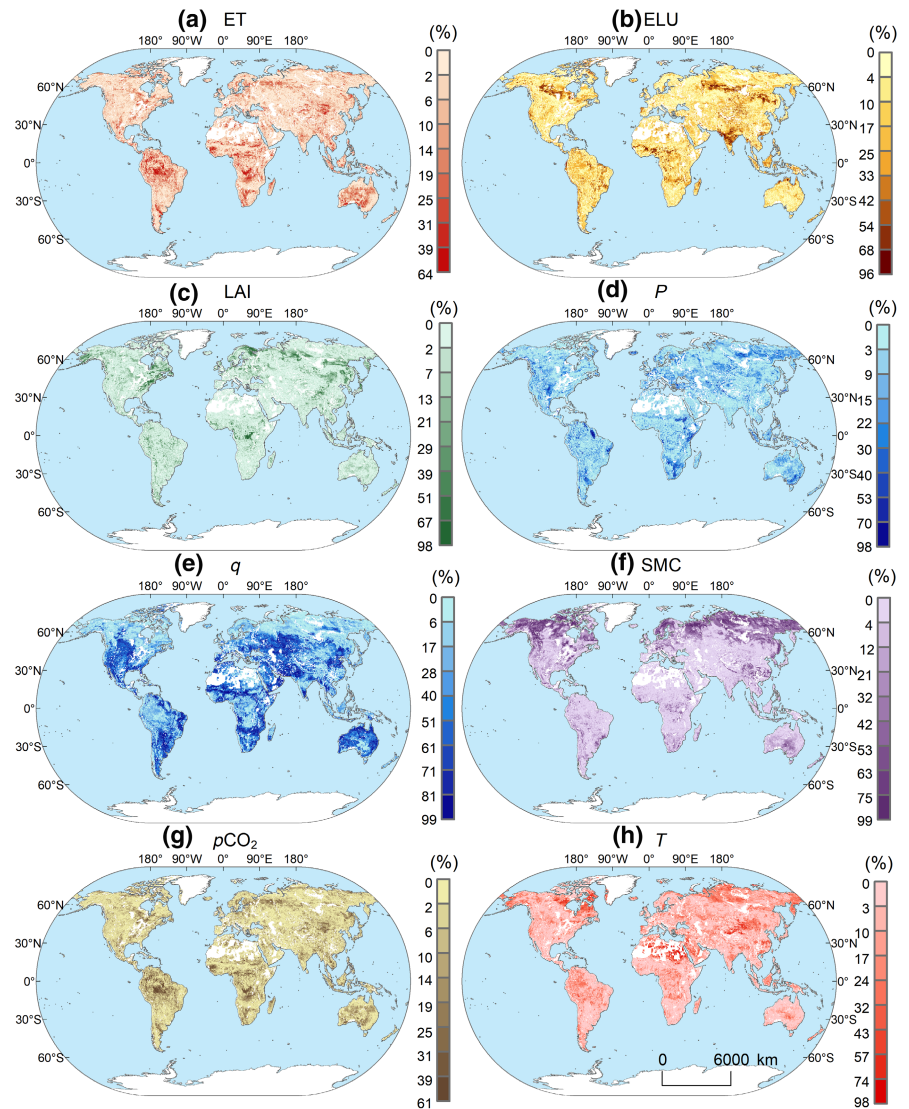
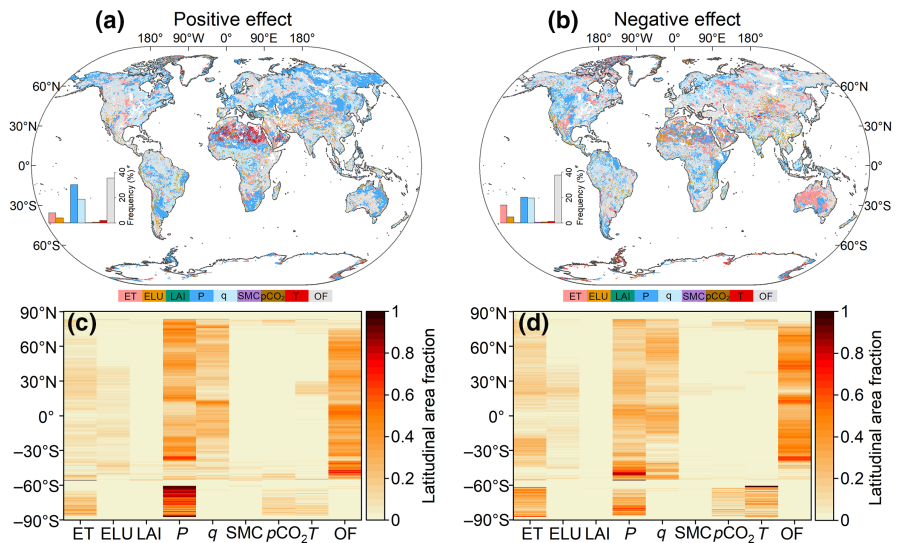


FIGURE 5 Spatial distribution and latitudinal contribution of different factors affecting the global silicate weathering carbon-sink flux (SCSF_α). (a) Positive effect of main factors on SCSF_α trends. (b) Negative effect of main factors on SCSF_α trends. (c) The latitudinal percentage of different factors in positive effect regions. (d) The latitudinal percentage of different factors in negative effect regions [Colour figure can be viewed at wileyonlinelibrary.com]



all, due to shortcomings in the quantity and quality of the compiled hydrochemistry monitoring data, most of the previous studies were multi-year average estimations of global silicate weathering carbon sinks (Table S4). This study combined the long-term global

hydro-chemistry database and hydro-meteorological data sets, and mapped a long-time series distribution map of the global silicate weathering carbon-sink flux. Simultaneously, most of the previous studies used the temperature stream model, inversion model,

numerical empirical model, and the method of multivariate linear regression. In the estimation process of this study, based on the relevant study by Hartmann et al. (2014b), a first-order model related factors was selected. We used the machine learning method to model and predict FHCO_3^- . In addition to some main factors (q, P, T, ET, LAI, ELU, and soil shielding), we also comprehensively considered other factors, such as SMC and pCO_2 , which were considered as critical factors affecting the weathering process. Due to the lack of data sets for soil pH and soil organic carbon content on the spatial grid scale of long-time series, these two data types were not considered in this study.

In addition, this study was different from previous studies in estimating the global area proportion of silicate rocks. The latest lithology data was used in this study, which was also applied to the estimation of the rock weathering rate (Gong et al., 2021; Xi et al., 2021). However, in this study, the proportion of carbonate in the main silicate lithology (SM, SS, SU) was excluded, and the final proportion of area reduction worldwide was 8.1%. It is worth noting that due to the limitation of lithology, this study did not completely exclude the distribution of trace carbonate in silicate rocks. Instead, we subtracted the effect of trace carbonate in the estimation process of total flux. Furthermore, there was a slight difference in the calculation of the total flux of the weathering carbon sink of silicate rock. In the study by Moon et al. (2014) and Hilley and Porder (2008), only Ca and Mg silicate weathering carbon sinks were considered, and the average values of their total flux were $143.22 \text{ Tg C yr}^{-1}$ and $65.5 \text{ Tg C yr}^{-1}$, respectively. In this study, we assumed that bicarbonate ions produced by the chemical weathering of silicate rocks were in equilibrium with the main cations (Ca, Mg, Na, and K), and the final calculated total flux was $167.56 \text{ Tg C yr}^{-1}$. Because the spatial data of the main factors collected were from the high-resolution data ($0.25^\circ \times 0.25^\circ$), the spatial-temporal resolution of the global silicate rock carbon sink was higher than that of the previous studies. This was of great significance for improving the simulation accuracy of the carbon sink and revealing the feedback between carbon and climate in the future.

4.2 | Verification of the accuracy of the inversion model

In this study, a single verification index between the simulation results based on the RF and observation data showed that Spearman $R = 0.68$, RMSE = 6.53, MAE = 4.21 (Figure 6a,b). This preliminarily illustrated the validity of the FHCO_3^- inversion results and showed that the inversion model could be used for effective simulation on the spatial grid scale. In addition, we also recognized the need to implement accuracy verification on the spatial patterns. Unlike traditional indicators that only focus on a single aspect, we used the latest multi-component spatial performance metric, namely SPAEF, to verify the spatial validity of the prediction results. This indicator can provide relatively reliable bias insensitive pattern information, even for two variables with different units, and it can also complete

the task of comparing complex spatial patterns (Koch et al., 2018). We found that the result of the SPAEF model could reach 0.33 (Figure 6d,e) and that the observed and simulated values in the histogram match well. All of these findings illustrated the relative reliability of the simulation results on the FHCO_3^- on the spatial grid scale. At the same time, we evaluated the relative importance of predictors in the FHCO_3^- based on RF inversion (Figure 6c). It was mainly found that the three factors of SMC, q, and LAI were more important than other environmental variables. Among them, SMC had the highest relative importance among all factors, which also reflected the role and value of this factor as an important predictor of FHCO_3^- inversion (Godderis et al., 2009). The importance of ET was the weakest among all factors, indicating that this factor did not increase in the mean error MSE, that is, in a statistical sense, this factor was equivalent to a random predictor variable.

4.3 | Comparison of physical erosion rate before and after improvement and its effectiveness

Physical erosion facilitates the chemical weathering process by accelerating the exposure of fresh rocks and keeping the weatherable minerals away from saturation (Gabet, 2007). Based on the two types of global land-use coordination data (high-value and low-value data) from 1950 to 2014, we revised the physical erosion rate in this study, and their average values were $164.49 \text{ t km}^{-2} \text{ yr}^{-1}$ (high value) and $164.75 \text{ t km}^{-2} \text{ yr}^{-1}$ (low value). The average ELU calculated for the high value of the land-use coordination data was slightly lower than that calculated for the low value data. Compared with the average value before correction, the ELU was reduced by $10.64\text{--}10.90 \text{ t km}^{-2} \text{ yr}^{-1}$, and the accuracy was improved by about 6%. This was mainly due to the difference between construction land and cultivated land in the two sets of land-use data, that is, the area percentages of these two types of land-use types in the high value data of land use were higher than the corresponding area percentages in the low value data of land use. Although there was little change in the average following the improvement in the physical erosion rate, the spatial distribution of the global physical erosion rate was closer to the actual observational data when considering changes in land-use patterns (Table S5). However, in view of the fact that the differences between the two sets ELU data (high and low) were small, there was no obvious difference in spatial distribution (Figure S17). Therefore, this study took the average of the two as the final physical erosion factor in this article.

To verify the accuracy and reliability of the improved global ELU, we compared the total ELU estimated in this study with previous related studies. On a global scale, the average ELU of this study ($164.62 \text{ t km}^{-2} \text{ yr}^{-1}$) was basically within the same order of magnitude as the previous studies ($129.53\text{--}179.19 \text{ t km}^{-2} \text{ yr}^{-1}$) (Table S5). However, despite using the same model (BQART model), the ELU in this study was slightly higher than that in the study by Maffre et al. (2018) ($156.00 \text{ t km}^{-2} \text{ yr}^{-1}$). This was mainly because of the difference in the accuracy of the simulated data. Maffred et al. (2018) used the

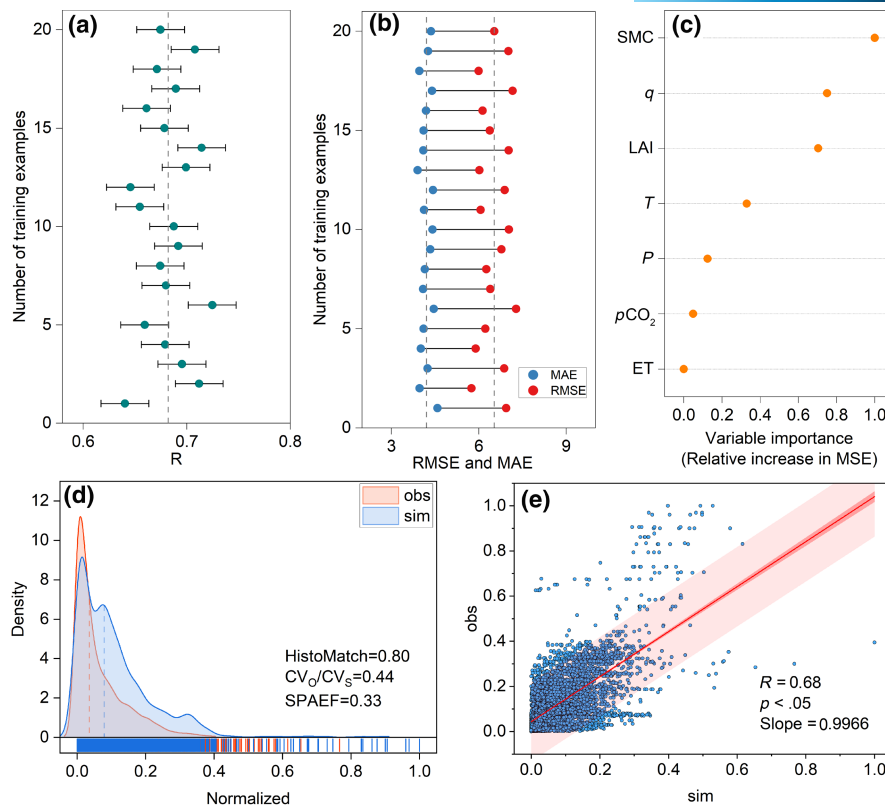


FIGURE 6 Accuracy verification of random forest model and relative importance of variables. (a) Spearman correlation coefficient (R) between model prediction samples and training samples. (b) Root mean square error of the model (RMSE) and mean absolute error (MAE). (c) Relative importance of variables (Relative increase in mean squared error (MSE)). Surface soil moisture content (SMC), Runoff (q), Leaf area index (LAI), Temperature (T), Precipitation (P), Partial pressure of soil carbon dioxide ($p\text{CO}_2$), and Evapotranspiration (ET). (d) Probability density distribution of observed values (obs) and simulated values (sim). The dotted lines in the figure refer to the median distribution of the observed and simulated values. HistoMatch refers to histogram match. (e) Scatter plot of obs and sim. In addition, the vertical dashed lines in (a) and (b) refer to the distribution of the mean values, and CV_o/CV_s and SPAEF in (d) are the spatial validity index and the final evaluation result of the index, respectively [Colour figure can be viewed at [wileyonlinelibrary.com](https://onlinelibrary.wiley.com)]

CRU database (1°), while we used the latest CMIP6 data (0.25°). In addition, based on the assumed rock density of 2.7 kg m^{-3} , we calculated that the global physical erosion thickness was 6.10 cm ka^{-1} , which is also within the range reported by previous studies ($4.80\text{--}6.64 \text{ cm ka}^{-1}$). On the catchment scale, the estimated magnitude of this study was generally close to the existing actual monitoring data (78 major river basins) (Milliman, 1995; Milliman & Farnsworth, 2011; Milliman & Syvitski, 1991), and the fitting effect of the two was better ($R^2 = 0.83$) (Figure S18). In addition, we compared the results of this study with the ^{10}Be -derived physical erosion rate estimates (cosmogenic radionuclide) (Portenga & Bierman, 2011). ^{10}Be produced in situ is mainly extracted from high-purity quartzite. The physical erosion rate calculated using this isotope is significantly different from that of this study. However, we found that the results of the two calculations also have a good fitting effect within the error range ($R^2 = 0.50$) (Figure S18). These observations illustrate the relative reliability of the ELU calculated in this study, which can be used to estimate the global silicate weathering carbon sink.

In addition, the ELU in this study was converted into a soil shielding factor, and based on this, the SCSF_α was calculated. To further reveal the effectiveness of ELU, we compared the improved

SCSF_α with the SCSF result calculated by the original soil shielding coefficient and compared them in the different silicate rock types. The improved SCSF_α ($1.39 \text{ t C km}^{-2} \text{ yr}^{-1}$) was significantly lower than the pre-improved SCSF ($1.65 \text{ t C km}^{-2} \text{ yr}^{-1}$), and the average flux was reduced by 16%. In addition, we selected 10,000 random points and analyzed the correlation between the improved SCSF_α and the SCSF before improvement (Figure S19), and found that the two had a better correlation ($R = 0.77$). However, in the low-value area and the high-value area, there were obvious differences before and after the improvement. After the improvement, the flux value in the low-value area increased, and the flux value in the high-value area decreased and showed similar characteristics to different silicate rock types. The difference between in the values before and after the improvement was mainly because the original soil shielding factor only considered two shielding factors, namely 0.1 and 1, which respectively represented the area affected by the soil shielding and the area not affected by the soil shielding. In this study, the numerical range of the soil shielding factor converted from ELU was between 0.5 and 1. Therefore, on the spatial grid scale, for some areas where the ELU was low and the developed soil layers were thicker, the SCSF_α was overestimated. However,

for some areas where the ELU was slower and the soil layer was thinner, that is, restricted by chemical weathering, the silicate weathering rate was more reasonable or effective than that before the improvement.

4.4 | Research shortcomings and future prospects

We took into account the important impact of land-use change on the ELU and attempted to convert it into the soil shielding factor for the first time. We re-estimated the high-resolution global silicate weathering carbon sink from 1950 to the end of this century and we identified and quantified the main control regions of different factors spatially. We strengthened the understanding of the formation process from of carbon sinks global silicate weathering and provided scientific insights for the effective development of future research on enhancing silicate weathering carbon sinks.

However, there were some shortcomings to this study, which need consideration in future research. First, to comprehensively consider all sources of uncertainties in the calculation of global silicate weathering carbon sinks, we used the Monte Carlo error propagation method for uncertainty analysis (Figure S20). The final calculated $SCSF_{\alpha}$ cumulative error was about $0.81 \text{ t C km}^{-2} \text{ yr}^{-1}$. On the one hand, the uncertainties come from the errors of the data sources. It is undeniable that the slope gradient calculated based on global 30 arc second elevation underestimates the physical erosion rate to a certain extent. Due to the nonlinear relationship between slope and physical erosion rate, this effect will decrease with an improvement of in data resolution (Larsen et al., 2014). Although CMIP6 product data have a higher resolution through improved dynamic processes, and SSPs have been applied to future climate change simulations. Compared with the CMIP5 data, these data have been improved to some extent, but there are also certain differences between different models (Chen et al., 2020b). Therefore, the error in the CMIP6 data becomes a potential source of uncertainty. At the same time, the hydro-chemistry monitoring database used in this study is one of the most complete water quality monitoring databases published, but the temporal scale and other aspects need to be further updated and improved. On the other hand, there are errors caused by the inversion of FHCO_3^- and the calculation of the soil shielding factor in the estimation method, as well as the deviation of the RCO_2 factor itself. The error contributed by RCO_2 may be the main one. Therefore, in the future research, the accurate quantification of RCO_2 under different lithologies will become an important direction. Second, some other factors (such as residence time, secondary minerals, mineral age, groundwater level, landslide, and glacier melting) are also considered to be important for the chemical weathering of silicate rocks (Torres et al., 2017). However, it is difficult to achieve effective spatialization for these impact factors, and their contribution is also controversial (Bufe et al., 2021). Some evidence suggests that glaciation in high latitudes promotes silicate chemical weathering by increasing the physical erosion rate (Koppes & Montgomery,

2009). In this study, these impact factors have been temporarily unified as residual factors in this study.

In the future, to actively cope with the challenge of global warming, it is necessary to strengthen the spatial simulation research of silicate weathering carbon sinks. At the same time, on the basis of identifying the main control regions of different factors on the silicate weathering carbon sink, the study on the spatial correlation and interaction between climate change and biological organisms on silicate weathering carbon sinks will become a meaningful direction to study the carbon sink regulation mechanism of silicate weathering at a regional scale.

5 | CONCLUSIONS

We quantitatively estimated the global silicate weathering carbon-sink flux ($SCSF_{\alpha}$) from 1950 to 2100 based on the global river chemistry database and hydro-meteorological data sets with improved first-order model and non-parametric methods. We found that the total $SCSF_{\alpha}$ was $155.80 \pm 90 \text{ Tg C yr}^{-1}$ in present period, which was expected to increase by approximately 12.13% by the end of this century. Although more than half of the global $SCSF_{\alpha}$ showed an upward trend, about 43% might show a downward trend, which was mainly controlled by runoff and precipitation factors on the spatial grid scale. There was a significant negative partial correlation between LAI and silicate weathering carbon sink flux due to the differences between the vegetation types. In the future, it is necessary to deeply explore the spatial correlation and interaction between climate change and biological organisms on the silicate weathering carbon sinks, which is valuable for the understanding of the role of silicate chemical weathering in the global carbon cycle.

ACKNOWLEDGMENTS

This research work was supported jointly by the Western Light Cross-team Program of Chinese Academy of Sciences (No. xzbzgzdsys-202101), National Natural Science Foundation of China (No. 42077455), Western Light Talent Program (Category A) (No. 2018-99), Strategic Priority Research Program of the Chinese Academy of Sciences (No. XDB40000000 & No. XDA23060100), Science and Technology Program of Guizhou Province (No. 2022-198), Opening Fund of the State Key Laboratory of Environmental Geochemistry (No. SKLEG2022206 & SKLEG2022208). We thank LetPub (www.letpub.com) for its linguistic assistance during the preparation of this manuscript.

CONFLICT OF INTEREST



The authors declare no real or perceived financial conflicts of interests.

ORCID

Chaojun Li  <https://orcid.org/0000-0001-9326-9743>

Xiaoyong Bai  <https://orcid.org/0000-0001-9705-5574>

Fei Chen  <https://orcid.org/0000-0003-1417-0898>

Sirui Zhang  <https://orcid.org/0000-0003-1259-745X>
 Lian Xiong  <https://orcid.org/0000-0001-5087-5639>
 Chaochao Du  <https://orcid.org/0000-0001-6964-0944>

REFERENCES

- Achard, F., Eva, H. D., Mayaux, P., Stibig, H. J., & Belward, A. (2004). Improved estimates of net carbon emissions from land cover change in the tropics for the 1990s. *Global Biogeochemical Cycles*, 18(2), GB2008. <https://doi.org/10.1029/2003GB002142>
- Amiotte Suchet, P., Probst, J. L., & Ludwig, W. (2003). Worldwide distribution of continental rock lithology: Implications for the atmospheric/soil CO₂ uptake by continental weathering and alkalinity river transport to the oceans. *Global Biogeochemical Cycles*, 17(2), 1038–1051. <https://doi.org/10.1029/2002GB001891>
- Bastin, J. F., Finegold, Y., Garcia, C., Mollicone, D., Rezende, M., Routh, D., & Crowther, T. (2019). The global tree restoration potential. *Science*, 365, 76–79. <https://doi.org/10.1126/science.aax0848>
- Beaulieu, E., Goddérís, Y., Donnadiou, Y., Labat, D., & Roelandt, C. (2012). High sensitivity of the continental-weathering carbon dioxide sink to future climate change. *Nature Climate Change*, 2(5), 346–349. <https://doi.org/10.1038/nclimate1419>
- Berner, R. (2006). A combined model for Phanerozoic atmospheric O₂ and CO₂. *Geochimica et Cosmochimica Acta*, 70, 5653–5664. <https://doi.org/10.1016/j.gca.2005.11.032>
- Berner, R., & Caldeira, K. (1997). The need for mass balance and feedback in the geochemical carbon cycle. *Geology*, 25, 955–956. [https://doi.org/10.1130/0091-7613\(1997\)0252.3.CO;2](https://doi.org/10.1130/0091-7613(1997)0252.3.CO;2)
- Berner, R. A., Lasaga, A. C., & Garrels, R. M. (1983). Carbonate-silicate geochemical cycle and its effect on atmospheric carbon dioxide over the past 100 million years. *American Journal of Science*, 283(7), 641–683. <https://doi.org/10.2475/ajs.283.7.641>
- Börker, J., Hartmann, J., Romero-Mujalli, G., & Li, G. (2019). Aging of basalt volcanic systems and decreasing CO₂ consumption by weathering. *Earth Surface Dynamics*, 7(1), 191–197. <https://doi.org/10.5194/esurf-7-191-2019>
- Borrelli, P., Robinson, D., Panagos, P., Lugato, E., Yang, J., Alewell, C., & Ballabio, C. (2020). Land use and climate change impacts on global soil erosion by water (2015–2070). *Proceedings of the National Academy of Sciences*, 117, 1–8. <https://doi.org/10.1073/pnas.2001403117>
- Breiman, L. (2001). Random forests. *Machine Learning*, 45, 5–32. <https://doi.org/10.1023/A:1010933404324>
- Brook, G., Folkoff, M., & Box, E. (1983). A world model of soil carbon dioxide: A reply. *Earth Surface Processes and Landforms*, 8, 79–88. <https://doi.org/10.1002/esp.3290080108>
- Bufe, A., Hovius, N., Emberson, R., Caves Rugenstein, J., Galy, A., Hassenruck-Gudipati, H., & Chang, J. (2021). Co-variation of silicate, carbonate and sulfide weathering drives CO₂ release with erosion. *Nature Geoscience*, 14, 211–216. <https://doi.org/10.1038/s41561-021-00714-3>
- Calmels, D., Gaillardet, J., Brenot, A., & France-Lanord, C. (2007). Sustained sulfide oxidation by physical erosion processes in the Mackenzie River basin: Climatic perspectives. *Geology*, 35, 1003–1006. <https://doi.org/10.1130/G24132A.1>
- Cao, J., Wu, X., Huang, F., Hu, B., Groves, C., Yang, H., & Zhang, C. (2018). Global significance of the carbon cycle in the karst dynamic system: evidence from geological and ecological processes. *China Geology*, 1(1), 17–27. <https://doi.org/10.31035/cg2018004>
- Chen, C., Li, D., Li, Y., Piao, S., Wang, X., Huang, M., & Myneni, R. (2020a). Biophysical impacts of Earth greening largely controlled by aerodynamic resistance. *Science Advances*, 6, eabb1981. <https://doi.org/10.1126/sciadv.abb1981>
- Chen, H., Sun, J., Lin, W., & Xu, H. (2020b). Comparison of CMIP6 and CMIP5 models in simulating climate extremes. *Science Bulletin*, 65, 1415–1418. <https://doi.org/10.1016/j.scib.2020.05.015>
- Cotton, J., Cerling, T., Hoppe, K., Mosier, T., & Still, C. (2016). Climate, CO₂, and the history of North American grasses since the Last Glacial Maximum. *Science Advances*, 2, e1501346. <https://doi.org/10.1126/sciadv.1501346>
- Dahlgren, R., Ugolini, F., & Casey, W. (1999). Field weathering rates of Mt. St. Helens tephra. *Geochimica et Cosmochimica Acta*, 63, 587–598. [https://doi.org/10.1016/S0016-7037\(99\)00067-8](https://doi.org/10.1016/S0016-7037(99)00067-8)
- de la Fuente, A., Bing, N., Hoeschele, I., & Mendes, P. (2005). Discovery of meaningful associations in genomic data using partial correlation coefficients. *Bioinformatics (Oxford, England)*, 20, 3565–3574. <https://doi.org/10.1093/bioinformatics/bth445>
- Demirel, M., Mai, J., Mendiguren González, G., Koch, J., Samaniego, L., & Stisen, S. (2018). Combining satellite data and appropriate objective functions for improved spatial pattern performance of a distributed hydrologic model. *Hydrology and Earth System Sciences*, 22, 1299–1315. <https://doi.org/10.5194/hess-22-1299-2018>
- Deng, Y., Wang, S., Bai, X., Luo, G., Wu, L., Cao, Y., & Tian, S. (2020). Variation trend of global soil moisture and its cause analysis. *Ecological Indicators*, 110, 105939. <https://doi.org/10.1016/j.ecoli.2019.105939>
- Dessert, C., Dupré, B., Gaillardet, J., François, L. M., & Allègre, C. J. (2003). Basalt weathering laws and the impact of basalt weathering on the global carbon cycle. *Chemical Geology*, 202(3), 257–273. <https://doi.org/10.1016/j.chemgeo.2002.10.001>
- Erskine, W., Mahmoudzadeh, A., & Myers, C. (2002). Land use effects on sediment yields and soil loss rates in small basins of Triassic sandstone near Sydney, NSW, Australia. *Catena*, 49, 271–287. [https://doi.org/10.1016/S0341-8162\(02\)00065-6](https://doi.org/10.1016/S0341-8162(02)00065-6)
- Eyring, V., Bony, S., Meehl, G., Senior, C., Stevens, B., Ronald, S., & Taylor, K. (2016). Overview of the coupled model intercomparison project phase 6 (CMIP6) experimental design and organization. *Geoscientific Model Development*, 9, 1937–1958. <https://doi.org/10.5194/gmd-9-1937-2016>
- Ferrier, K., & Kirchner, J. (2008). Effects of physical erosion on chemical denudation rates: A numerical modeling study of soil-mantled hillslopes. *Earth and Planetary Science Letters*, 272, 591–599. <https://doi.org/10.1016/j.epsl.2008.05.024>
- Gabet, E. J. (2007). A theoretical model coupling chemical weathering and physical erosion in landslide-dominated landscapes. *Earth and Planetary Science Letters*, 264(1), 259–265. <https://doi.org/10.1016/j.epsl.2007.09.028>
- Gaillardet, J., Calmels, D., Romero-Mujalli, G., Zakharova, E., & Hartmann, J. (2019). Global climate control on carbonate weathering intensity. *Chemical Geology*, 527, 118762. <https://doi.org/10.1016/j.chemgeo.2018.05.009>
- Gaillardet, J., Dupré, B., Louvat, P., & Allègre, C. J. (1999). Global silicate weathering and CO₂ consumption rates deduced from the chemistry of large rivers. *Chemical Geology*, 159(1), 3–30. [https://doi.org/10.1016/S0009-2541\(99\)00031-5](https://doi.org/10.1016/S0009-2541(99)00031-5)
- Gislason, S., Oelkers, E., Eiriksdottir, E., Kardjilov, M., Gisladóttir, G., Sigfusson, B., & Oskarsson, N. (2009). Direct evidence of the feedback between climate and weathering. *Earth and Planetary Science Letters*, 277, 213–222. <https://doi.org/10.1016/j.epsl.2008.10.018>
- Godderis, Y., Brantley, S., François, L., Schott, J., Pollard, D., Déqué, M., & Dury, M. (2013). Rates of consumption of atmospheric CO₂ through the weathering of loess during the next 100 yr of climate change. *Biogeosciences*, 10, 135–148. <https://doi.org/10.5194/bg-10-135-2013>
- Godderis, Y., Donnadiou, Y., Carretier, S., Aretz, M., Dera, G., Macouin, M., & Regard, V. (2017). Onset and ending of the late Palaeozoic ice age triggered by tectonically paced rock weathering. *Nature Geoscience*, 10, 382–386. <https://doi.org/10.1038/ngeo2931>
- Godderis, Y., Roelandt, C., Schott, J., Pierret, M. C., & François, L. (2009). Towards an integrated model of weathering, climate, and biospheric processes. *Reviews in Mineralogy and Geochemistry*, 70, 411–434. <https://doi.org/10.2138/rmg.2009.70.9>

- Goldsmith, S., Harmon, R., Lyons, W., Harmon, B., Ogden, F., & Gardner, C. (2015). Evaluation of controls on silicate weathering in tropical mountainous rivers: Insights from the Isthmus of Panama. *Geology*, 43, 563–566. <https://doi.org/10.1130/G36082.1>
- Gong, S., Wang, S., Bai, X., Luo, G., Wu, L., Chen, F., & Zeng, C. (2021). Response of the weathering carbon sink in terrestrial rocks to climate variables and ecological restoration in China. *Science of the Total Environment*, 750, 141525. <https://doi.org/10.1016/j.scitotenv.2020.141525>
- Gwiazda, R., & Broecker, W. (1994). The separate and combined effects of temperature, soil pCO₂, and organic acidity on silicate weathering in the soil environment: Formulation of a model and results. *Global Biogeochemical Cycles*, 8, 141–155. <https://doi.org/10.1029/94GB00491>
- Harris, N., Gibbs, D., Baccini, A., Birdsey, R., de Bruin, S., Farina, M., & Tyukavina, A. (2021). Global maps of twenty-first century forest carbon fluxes. *Nature Climate Change*, 11, 234–240. <https://doi.org/10.1038/s41558-020-00976-6>
- Hartmann, J. (2009). Bicarbonate-fluxes and CO₂-consumption by chemical weathering on the Japanese Archipelago – Application of a multi-lithological model framework. *Chemical Geology*, 265(3), 237–271. <https://doi.org/10.1016/j.chemgeo.2009.03.024>
- Hartmann, J., Dürr, H. H., Moosdorf, N., Meybeck, M., & Kempe, S. (2012). The geochemical composition of the terrestrial surface (without soils) and comparison with the upper continental crust. *International Journal of Earth Sciences*, 101(1), 365–376. <https://doi.org/10.1007/s00531-010-0635-x>
- Hartmann, J., Lauerwald, R., & Moosdorf, N. (2014a). A brief overview of the GLOBAL River chemistry database, GLORICH. *Procedia Earth and Planetary Science*, 10, 23–27. <https://doi.org/10.1016/j.proeps.2014.08.005>
- Hartmann, J., & Moosdorf, N. (2011). Chemical weathering rates of silicate-dominated lithological classes and associated liberation rates of phosphorus on the Japanese Archipelago—Implications for global scale analysis. *Chemical Geology*, 287, 125–157. <https://doi.org/10.1016/j.chemgeo.2010.12.004>
- Hartmann, J., & Moosdorf, N. (2012). The new global lithological map database (GLiM): A representation of rock properties at the Earth surface. *Geochemistry Geophysics Geosystems*, 13, Q12004. <https://doi.org/10.1029/2012GC004370>
- Hartmann, J., Moosdorf, N., Lauerwald, R., Hinderer, M., & West, A. J. (2014b). Global chemical weathering and associated P-release – The role of lithology, temperature and soil properties. *Chemical Geology*, 363, 145–163. <https://doi.org/10.1016/j.chemgeo.2013.10.025>
- Herrnegger, M., Feigl, M., Karsten, S., & Klotz, D. (2020). Function space optimization: A symbolic regression method for estimating parameter transfer functions for hydrological models. *Water Resources Research*, 56, e2020WR027385. <https://doi.org/10.1029/2020WR027385>
- Hilley, G., & Porder, S. (2008). A framework for predicting global silicate weathering and CO₂ drawdown rates over geologic timescales. *Proceedings of the National Academy of Sciences of the United States of America*, 105, 16855–16859. <https://doi.org/10.1073/pnas.0801462105>
- Hilton, R., & West, A. J. (2020). Mountains, erosion and the carbon cycle. *Nature Reviews Earth & Environment*, 1, 284–299. <https://doi.org/10.1038/s43017-020-0058-6>
- Ibarra, D. E., Caves, J. K., Moon, S., Thomas, D. L., Hartmann, J., Chamberlain, C. P., & Maher, K. (2016). Differential weathering of basaltic and granitic catchments from concentration–discharge relationships. *Geochimica et Cosmochimica Acta*, 190, 265–293. <https://doi.org/10.1016/j.gca.2016.07.006>
- Kanzaki, Y., Brantley, S. L., & Kump, L. R. (2020). A numerical examination of the effect of sulfide dissolution on silicate weathering. *Earth and Planetary Science Letters*, 539, 116239. <https://doi.org/10.1016/j.epsl.2020.116239>
- Keene, W., Pszeny, A., Galloway, J., & Hawley, M. (1986). Sea salt correction and interpretation of constituent ratios in marine precipitation. *Journal of Geophysical Research*, 91, 6647–6658. <https://doi.org/10.1029/JD091iD06p06647>
- Kendall, M., & Stuart, A. S. (1968). The advanced theory of statistics. *The Statistician*, 18, 163. <https://doi.org/10.2307/2986781>
- Koch, J., Demirel, M., & Stisen, S. (2018). The SPAtial Efficiency metric (SPAEF): Multiple-component evaluation of spatial patterns for optimization of hydrological models. *Geoscientific Model Development*, 11, 1873–1886. <https://doi.org/10.5194/gmd-11-1873-2018>
- Kohavi, R. (1995). *A study of cross-validation and bootstrap for accuracy estimation and model selection* (Vol. 14). Morgan Kaufmann Publishers Inc.
- Koppes, M., & Montgomery, D. (2009). The relative efficacy of fluvial and glacial erosion over modern to orogenic timescales. *Nature Geoscience*, 2, 644–647. <https://doi.org/10.1038/ngeo616>
- Kuhn, M. (2008). Building predictive models in R using the caret package. *Journal of Statistical Software*, 28, 26. <https://doi.org/10.18637/jss.v028.i05>
- Kump, L., Brantley, S., & Arthur, M. (2000). Chemical weathering, atmospheric CO₂, and climate. *Annual Review of Earth and Planetary Sciences*, 28, 611–667. <https://doi.org/10.1146/annurev.earth.28.1.611>
- Kuzyakov, Y. (2006). Sources of CO₂ efflux from soil and review of partitioning methods. *Soil Biology and Biochemistry*, 38, 425–448. <https://doi.org/10.1016/j.soilbio.2005.08.020>
- Larsen, I. J., Almond, P. C., Eger, A., Stone, J. O., Montgomery, D. R., & Malcolm, B. (2014). Rapid soil production and weathering in the southern Alps, New Zealand. *Science*, 343(6171), 637. <https://doi.org/10.1126/science.1244908>
- Li, D., Jacobson, A., & McInerney, D. (2014). A reactive-transport model for examining tectonic and climatic controls on chemical weathering and atmospheric CO₂ consumption in granitic regolith. *Chemical Geology*, 365, 30–42. <https://doi.org/10.1016/j.chemgeo.2013.11.028>
- Li, H., Wang, S., Bai, X., Cao, Y., & Wu, L. (2019). Spatiotemporal evolution of carbon sequestration of limestone weathering in China. *Science China Earth Sciences*, 62(6), 974–991. <https://doi.org/10.1007/s11430-018-9324-2>
- Li, H., Wang, S., Bai, X., Luo, W., Tang, H., Cao, Y., & Wang, M. (2018). Spatiotemporal distribution and national measurement of the global carbonate carbon sink. *Science of the Total Environment*, 643, 157–170. <https://doi.org/10.1016/j.scitotenv.2018.06.196>
- Li, X., Liu, J. P., Saito, Y., & Nguyen, V. (2017). Recent evolution of the Mekong Delta and the impacts of dams. *Earth-Science Reviews*, 175, 1–17. <https://doi.org/10.1016/j.earscirev.2017.10.008>
- Liu, J., & Han, G. (2020). Major ions and δ³⁴S_{SO₄ in Jiulongjiang River water: Investigating the relationships between natural chemical weathering and human perturbations. *Science of the Total Environment*, 724, 138208. <https://doi.org/10.1016/j.scitotenv.2020.138208>}
- Louvat, P., & Allègre, C. (1997). Present denudation rates on the island of Réunion determined by river geochemistry: Basalt weathering and mass budget between chemical and mechanical erosions. *Geochimica et Cosmochimica Acta*, 61, 3645–3669. [https://doi.org/10.1016/S0016-7037\(97\)00180-4](https://doi.org/10.1016/S0016-7037(97)00180-4)
- Luo, X., Bai, X., Tan, Q., Ran, C., Chen, H., Xi, H., & Tian, S. (2022). Particulate organic carbon exports from the terrestrial biosphere controlled by erosion. *Catena*, 209, 105815. <https://doi.org/10.1016/j.catena.2021.105815>
- Mackenzie, F., & Garrels, R. (1971). *Evolution of sedimentary rocks* (Vol. 101). Norton.
- Maffre, P., Ladant, J., Moquet, J., Carretier, S., Labat, D., & Godderis, Y. (2018). Mountain ranges, climate and weathering. Do orogens

- strengthen or weaken the silicate weathering carbon sink? *Earth and Planetary Science Letters*, 493, 174–185. <https://doi.org/10.1016/j.epsl.2018.04.034>
- Maher, K., & Chamberlain, C. P. (2014). Hydrologic regulation of chemical weathering and the geologic carbon cycle. *Science*, 343(6178), 1502. <https://doi.org/10.1126/science.1250770>
- Mann, H. (1945). Non-parametric test against trend. *Econometrica*, 13, 245–259. <https://doi.org/10.2307/1907187>
- Martin, A. N., Dosseto, A., May, J. H., Jansen, J. D., Kinsley, L. P. J., & Chivas, A. R. (2019). Sediment residence times in catchments draining to the Gulf of Carpentaria, northern Australia, inferred by uranium comminution dating. *Geochimica et Cosmochimica Acta*, 244, 264–291. <https://doi.org/10.1016/j.gca.2018.09.031>
- Meybeck, M., & Ragu, A. (2012). GEMS-GLORI world river discharge database. <https://doi.org/10.1594/PANGAEA.804574>
- Mielnick, P., & Dugas, W. (2000). Soil CO₂ flux in a tallgrass prairie. *Soil Biology & Biochemistry*, 32, 221–228. [https://doi.org/10.1016/S0038-0717\(99\)00150-9](https://doi.org/10.1016/S0038-0717(99)00150-9)
- Milliman, J. D. (1995). *River discharge to the sea a global river index (GLORI)*. IGBP-LOICZ Report.
- Milliman, J., & Farnsworth, K. (2011). *River discharge to the coastal ocean – A global synthesis*. Cambridge University Press.
- Milliman, J., & Syvitski, J. (1991). Geomorphic tectonic control of sediment discharge to ocean – The importance of small mountainous rivers. *Journal of Geology*, 100, 525–544. <https://doi.org/10.1086/629606>
- Moon, S., Chamberlain, C. P., & Hilley, G. E. (2014). New estimates of silicate weathering rates and their uncertainties in global rivers. *Geochimica et Cosmochimica Acta*, 134, 257–274. <https://doi.org/10.1016/j.gca.2014.02.033>
- Moosdorf, N., Hartmann, J., Lauerwald, R., Hagedorn, B., & Kempe, S. (2011). Atmospheric CO₂ consumption by chemical weathering in North America. *Geochimica et Cosmochimica Acta*, 75(24), 7829–7854. <https://doi.org/10.1016/j.gca.2011.10.007>
- Portenga, E., & Bierman, P. (2011). Understanding Earth's eroding surface with 10Be. *GSA Today*, 21, 4–10. <https://doi.org/10.1130/G111A.1>
- Raymond, P. A., Oh, N. H., Turner, R. E., & Broussard, W. (2008). Anthropogenically enhanced fluxes of water and carbon from the Mississippi River. *Nature*, 451(7177), 449–452. <https://doi.org/10.1038/nature06505>
- Reicosky, D., Gesch, R. W., Wagner, S., Gilbert, R. A., Wentz, C. D., & Morris, D. R. (2008). Tillage and wind effects on soil CO₂ concentrations in muck soils. *Soil and Tillage Research*, 99, 221–231. <https://doi.org/10.1016/j.still.2008.02.006>
- Roderick, M. L., Rotstain, L. D., Farquhar, G. D., & Hobbins, M. T. (2007). On the attribution of changing pan evaporation. *Geophysical Research Letters*, 34(17), L17403. <https://doi.org/10.1029/2007G1031166>
- Ruddiman, W. F. (1997). *Tectonic uplift and climate change*. Springer Science & Business Media.
- Sen, P. (1968). Estimates of the regression coefficient based on Kendall's Tau. *Journal of the American Statistical Association*, 63(324), 1379–1389. <https://doi.org/10.1080/01621459.1968.10480934>
- Song, F., Wang, S., Bai, X., Wu, L., Wang, J., Li, C., & Zhen, Q. (2022). A new indicator for global food security assessment: harvested area rather than cropland area. *Chinese Geographical Science*, 32(2), 204. <https://doi.org/10.1007/s11769-022-1264-6>
- Stallard, R. F. (1995). Tectonic, environmental, and human aspects of weathering and erosion: A global review using a steady-state perspective. *Annual Review of Earth and Planetary Sciences*, 23(1), 11–39. <https://doi.org/10.1146/annurev.earth.23.050195.000303>
- Suchet, P., & Probst, J. L. (1995). A global model for present-day atmospheric/soil CO₂ consumption by chemical erosion of continental rocks (GEM-CO₂). *Tellus Series B*, 47, 273–280. <https://doi.org/10.3402/tellusb.v47i1-2.16047>
- Syvitski, J. P. M., & Milliman, J. D. (2007). Geology, geography, and humans battle for dominance over the delivery of fluvial sediment to the Coastal Ocean. *Journal of Geology*, 115(1), 1–19. <https://doi.org/10.1086/509246>
- Taylor, L., Quirk, J., Thorley, R., Kharecha, P., Hansen, J., Ridgwell, A., & Beerling, D. (2015). Enhanced weathering strategies for stabilizing climate and averting ocean acidification. *Nature Climate Change*, 6, 402–406. <https://doi.org/10.1038/nclimate2882>
- Tian, S., Wang, S., Bai, X., Luo, G., Li, Q., Yang, Y., & Deng, Y. (2021). Global patterns and changes of carbon emissions from land use during 1992–2015. *Environmental Science and Ecotechnology*, 7, 100108. <https://doi.org/10.1016/j.ese.2021.100108>
- Torres, M., Moosdorf, N., Hartmann, J., Adkins, J., & West, A. J. (2017). Glacial weathering, sulfide oxidation, and global carbon cycle feedbacks. *Proceedings of the National Academy of Sciences*, 114, 201702953. <https://doi.org/10.1073/pnas.1702953114>
- Torres, M., West, A. J., Clark, K., Paris, G., Bouchez, J., Ponton, C., & Adkins, J. (2016). The acid and alkalinity budgets of weathering in the Andes-Amazon system: Insights into the erosional control of global biogeochemical cycles. *Earth and Planetary Science Letters*, 450, <https://doi.org/10.1016/j.epsl.2016.06.012>
- Torres, M. A., West, A. J., & Li, G. (2014). Sulphide oxidation and carbonate dissolution as a source of CO₂ over geological timescales. *Nature*, 507(7492), 346–349. <https://doi.org/10.1038/nature13030>
- Vicca, S., Goll, D. S., Hagens, M., Hartmann, J., Janssens, I. A., Neubeck, A., & Verbruggen, E. (2022). Is the climate change mitigation effect of enhanced silicate weathering governed by biological processes? *Global Change Biology*, 28(3), 711–726. <https://doi.org/10.1111/gcb.15993>
- Walker, J., Hays, P., & Kasting, J. (1981). A Negative feedback mechanism for the long-term stabilization of Earth's surface-temperature. *Journal of Geophysical Research Atmospheres*, 86, 9776–9782. <https://doi.org/10.1029/JC086iC10p09776>
- West, A. J. (2012). Thickness of the chemical weathering zone and implications for erosional and climatic drivers of weathering and for carbon-cycle feedbacks. *Geology*, 40, 811–814. <https://doi.org/10.1130/G33041.1>
- West, A. J., Galy, A., & Bickle, M. (2005). Tectonic and climatic controls on silicate weathering. *Earth and Planetary Science Letters*, 235(1), 211–228. <https://doi.org/10.1016/j.epsl.2005.03.020>
- White, A. F., & Blum, A. E. (1995). Effects of climate on chemical weathering in watersheds. *Geochimica et Cosmochimica Acta*, 59(9), 1729–1747. [https://doi.org/10.1016/0016-7037\(95\)00078-E](https://doi.org/10.1016/0016-7037(95)00078-E)
- Wilson, T. R. S. (1975). Salinity and the major elements of sea water. In J. P. Riley, & G. Skirrow (Eds.), *Chemical oceanography: Salinity and the major elements of sea water* (2 ed., Vol. 1, pp. 365–413). Academic Press.
- Wong, T. T. (2015). Performance evaluation of classification algorithms by k-fold and leave-one-out cross validation. *Pattern Recognition*, 48, 2839–2846. <https://doi.org/10.1016/j.patcog.2015.03.009>
- Xi, H., Wang, S., Bai, X., Tang, H., Luo, G., Li, H., & Luo, X. (2021). The responses of weathering carbon sink to eco-hydrological processes in global rocks. *Science of the Total Environment*, 788, 147706. <https://doi.org/10.1016/j.scitotenv.2021.147706>
- Yan, J., Li, J., Ye, Q., & Li, K. (2012). Concentrations and exports of solutes from surface runoff in Houzhai Karst Basin, southwest China. *Chemical Geology*, 304–305, 1–9. <https://doi.org/10.1016/j.chemgeo.2012.02.003>
- Yang, D., Kanae, S., Oki, T., Koike, T., & Musiak, K. (2003). Global potential soil erosion with reference to land use and climate changes. *Hydrological Processes*, 17, 2913–2928. <https://doi.org/10.1002/hyp.1441>
- Yang, Y., Wang, S., Bai, X., Tan, Q., Li, Q., Wu, L., & Deng, Y. (2019). Factors affecting long-term trends in global NDVI. *Forests*, 10(5), 372. <https://doi.org/10.3390/f10050372>
- Zeebe, R., & Caldeira, K. (2008). Close mass balance of long-term carbon fluxes from ice-core CO₂ and ocean chemistry records. *Nature Geoscience*, 1, 312–315. <https://doi.org/10.1038/ngeo185>

- Zeng, S., Liu, Z., & Kaufmann, G. (2019). Sensitivity of the global carbonate weathering carbon-sink flux to climate and land-use changes. *Nature Communications*, 10(1), 5749. <https://doi.org/10.1038/s41467-019-13772-4>
- Zhang, S., Bai, X., Zhao, C., Tan, Q., Luo, G., Cao, Y., & Liu, M. (2022a). Limitations of soil moisture and formation rate on vegetation growth in karst areas. *Science of the Total Environment*, 810, 151209. <https://doi.org/10.1016/j.scitotenv.2021.151209>
- Zhang, S., Bai, X., Zhao, C., Tan, Q., Luo, G., Wang, J., & Xi, H. (2021). Global CO₂ Consumption by silicate rock chemical weathering. Its past and future. *Earth's Future*, 9(5), e2020EF001938. <https://doi.org/10.1029/2020EF001938>
- Zhang, S., Bai, X., Zhao, C., Tan, Q., Luo, G., Wu, L., & Song, F. (2022b). China's carbon budget inventory from 1997 to 2017 and its challenges to achieving carbon neutral strategies. *Journal of Cleaner Production*, 347, 130966. <https://doi.org/10.1016/j.jclepro.2022.130966>

SUPPORTING INFORMATION

Additional supporting information may be found in the online version of the article at the publisher's website.

How to cite this article: Li, C., Bai, X., Tan, Q., Luo, G., Wu, L., Chen, F., Xi, H., Luo, X., Ran, C., Chen, H., Zhang, S., Liu, M., Gong, S., Xiong, L., Song, F., Xiao, B., & Du, C. (2022). High-resolution mapping of the global silicate weathering carbon sink and its long-term changes. *Global Change Biology*, 28, 4377–4394. <https://doi.org/10.1111/gcb.16186>